

AD629241

PHOTOVOLTAIC POWER SYSTEMS USING HIGH SOLAR ENERGY FLUXES

FINAL REPORT

CONTRACT NO. DA-28-043 AMC-00005(E)
DA TASK NO. IC6-22001-A-053-01

March 1, 1964 to November 30, 1965

CLEARINGHOUSE FOR FEDERAL SCIENTIFIC AND TECHNICAL INFORMATION		
Hardcopy	Microfiche	
\$3.00	\$0.75	73 PPI <i>ad</i>
ARCHIVE COPY		

U. S. Army Electronics Command
Fort Monmouth, New Jersey

Code 1

THE UNIVERSITY OF WISCONSIN
Engineering Experiment Station
Solar Energy Laboratory
Madison, Wisconsin

NOTICES

DISCLAIMERS

The findings in this report are not to be construed as an official Department of the Army position, unless so designated by other authorized documents.

The citation of trade names and names of manufacturers in this report is not to be construed as official Government indorsement or approval of commercial products or services referenced herein.

DISPOSITION

Destroy this report when it is no longer needed. Do not return it to the originator.

PHOTOVOLTAIC POWER SYSTEMS USING
HIGH SOLAR ENERGY FLUXES

FINAL REPORT

CONTRACT NO. DA-28-043 AMC-00005(E)

TECHNICAL GUIDELINES DATED OCTOBER 18, 1963

DA Task No. 1C6-22001-A-053-01

Report Date: December 30, 1965

Period: March 1, 1964 to Nov. 30, 1965

OBJECTIVE: Investigation of Methods for Producing
50 Watts of Electrical Power From a High
Solar Flux Photovoltaic System

Report Prepared by: P. Schoffer
W. Beckman

THE UNIVERSITY OF WISCONSIN
Engineering Experiment Station
Solar Energy Laboratory
Madison, Wisconsin

TABLE OF CONTENTS

LIST OF ILLUSTRATIONS	1
PURPOSE	3
PUBLICATIONS, LECTURES, REPORTS AND CONFERENCES	4
ABSTRACT	5
A. INTRODUCTION	6
B. CELL INVESTIGATION	8
1. Cell Optimization	8
2. Cell Performance and Conclusions	14
C. COOLING SYSTEM	17
1. Introduction	17
2. Cell Cooling System Design and Performance	20
3. Air Heat Exchanger	26
4. Pump and Motor	31
D. SOLAR REFLECTOR	39
E. ELECTRICAL CONTROL SYSTEM	42
F. ARRAY CONSTRUCTION	47
G. SYSTEM EXPERIMENTS	51
1. General Discussion	51
2. Electrical Measurements	53
H. CONCLUSIONS	59
I. RECOMMENDATIONS	60
APPENDIX	61
REFERENCES	67

LIST OF ILLUSTRATIONS

- FIGURE 1. System Schematic
- FIGURE 2. Computed Efficiency as a Function of Number of Gridlines Over 1 Cm at Various Input Fluxes.
- FIGURE 3. Computed Output Power as a Function of the Number of Gridlines Over 1 Cm, at Various Input Fluxes
- FIGURE 4. Grid Configuration
- FIGURE 5. Cell and Heatsink
- FIGURE 6. Typical Cell Efficiency Vs. Temperature
- FIGURE 7. Cell Heatsink Configuration
- FIGURE 8. $T_c - T_\infty$ for Various Pin Lengths and Water Flow Rates a Function of the Theoretical Cell Array Pump Power Requirements
- FIGURE 9. Experimental ($T_c - T_\infty$) Vs. Water Flow Rate for 3 Pin Lengths
- FIGURE 10. Air Heat Exchanger Performance
- FIGURE 11. Pump Flow Rate Vs. RPM
- FIGURE 12. Pump Power Vs. RPM
- FIGURE 13. Pump Component Power Vs. RPM
- FIGURE 14. Pump and Motor Characteristics at Zero Head
- FIGURE 15. Flux Distribution on Cell Array
- FIGURE 16. Cell Array Connection Box
- FIGURE 17. Front and Back Views of Cells and Frame
- FIGURE 18. Cell Array
- FIGURE 19. Overall View of System
- FIGURE 20. Array Current and Power Vs. Voltage at 40°C

FIGURE 21. Array Current and Power Vs. Voltage at 60°C

FIGURE 22. Array Current and Power Vs. Voltage at 47°C

FIGURE 1A Cell Equivalent Circuits

FIGURE 2A Rho Line

PURPOSE*

The purpose of this contract is the development of a 50-watt high-solar-flux photovoltaic power generation system for terrestrial use. Various solar cell parameters are to be experimentally investigated with the objective of obtaining a high efficiency at high solar concentration ratios. Various techniques for cooling the cells will be investigated analytically with the ultimate objective of obtaining the maximum net electrical power generation. A breadboard system (not necessarily an optimum design) will be constructed to experimentally determine the electrical output for appropriate ranges in operating conditions. A subsequent comparison of experimental results and analytical predictions will permit design of an optimized power generation facility.

*Quoted from Quarterly Reports.

PUBLICATIONS, LECTURES, REPORTS AND CONFERENCES

1. Publications, Lectures and Reports

Beckman, W., Schoffer, P. and Hartman, W., "A Photo-Voltaic Power System Using Concentrated Solar Energy." Paper presented at the Annual Meeting of the Solar Energy Society, Phoenix, Arizona, March 1965.

2. Conferences

On August 27, 1965 a meeting was held at the University of Wisconsin between E. Kittl and A. Herchakowski of USAECOM and P. Schoffer, J. Duffie and W. Beckman of the Solar Energy Laboratory. Progress on the construction of the breadboard system was discussed. The performance tests on the individual cooling system components were presented. The plans for the system tests were also discussed.

ABSTRACT

Experimental data is presented on the operation of a high solar flux power system. Using 18 one by two cm cells with 20 gridlines/cm and with a concentrated solar flux of about 25 W/cm^2 , the system produced 40 watts of electrical power. Approximately 5 of the 40 watts are necessary for the cooling system pump motor. The expected net output of 50 watts was not obtained due to low cell efficiencies and nonuniform flux distribution. Probable reasons for the low cell efficiencies are discussed and a method for obtaining a more uniform flux distribution is presented. Tests on the individual cooling system components are also presented.

A. INTRODUCTION

Most of the photovoltaic converters now in use employ silicon cells which operate at normal solar radiation levels near 90 milliwatts per square centimeter and have power outputs of about 12 milliwatts per square centimeter at these radiation levels. Silicon cells can also be used with a solar concentrator. Work done from 1962 to 1964 (1, 2) shows that cell outputs of over 1.5 watts/cm^2 can be obtained which permit the number of cells per watt to be reduced by a factor of 120 or more. Since the cost of the cells in most silicon cell power systems is a significant percentage of the total cost, it may be economically advantageous to use high solar concentration ratios.

In order to produce useful power from a high solar flux system, consideration must be given to methods of obtaining the desired solar flux, predicting the cell performance characteristics and maintaining the cells at a reasonably low temperature level. This report describes the design of a high flux power system and reports experimental measurements on the performance of the system. Also included are measurements of cell characteristics at high fluxes, predictions of the performance of other cell designs at these high fluxes and methods of cell cooling.

The primary system application is the charging of storage batteries with unattended operation over extended periods of time in a 49°C environment. In order to be independent of local conditions, the use of open system cooling such as might be obtained from a nearby water supply was not considered. Thus it is necessary to use a closed loop system as shown schematically in Figure 1. In this system, the thermal energy resulting from the concentrated solar energy absorbed by the cells is dissipated to

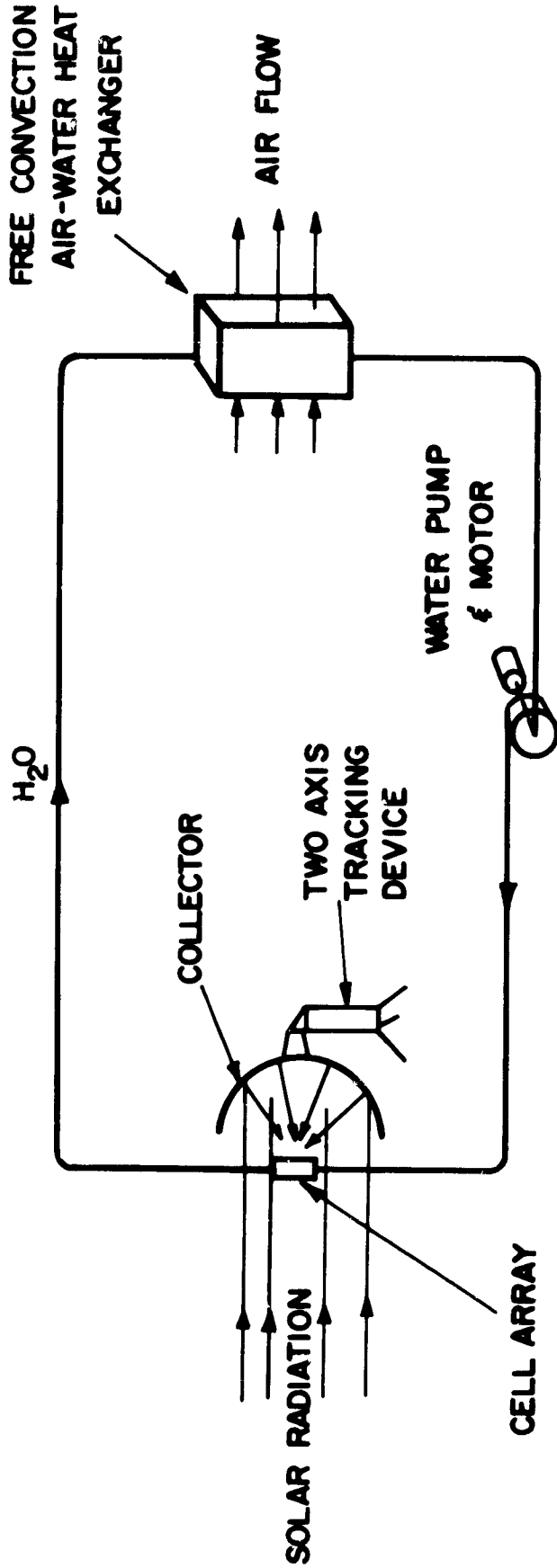


FIGURE 1. SYSTEM SCHEMATIC

cooling water which is continuously circulated by a small pump and motor. The thermal energy from the cooling water is then transferred to the atmosphere by a free convection finned-tube heat exchanger. The electrical power for the pump motor is supplied by the cells.

B. CELL INVESTIGATION

1. Cell Optimization

An earlier investigation (1) using ordinary cells with 3 gridlines/cm and high fluxes predicted that cells operating at solar fluxes between 14 and 28 watts/cm² have an optimum efficiency with about 15 gridlines per cm. This gridline pattern consists of a lengthwise central conductor with grids extending off the center to the edges. It was found that the extreme extrapolation from normally gridded cells to the densely gridded cells yielded higher efficiencies than could be experimentally obtained. This was due to the fact that the resistance perpendicular to the cells (grid resistance + bulk resistance + plating resistance) could not be accurately determined. That is, with the relatively large cell surface resistance of normally gridded cells, it is impossible to separate the perpendicular resistance from the total cell resistance. With experimental measurements using a denser grid pattern (15 gridlines per cm), the perpendicular resistance and surface resistance are of the same order of magnitude and can be separated. (See Appendix.)

Cells with fifteen gridlines/cm were cut in half and soldered on a water-cooled partially flattened copper tube. The cells were then mounted behind a flux distributor which was positioned at the focal spot of a 1.53 meter diameter searchlight mirror. With this system, fluxes up to 110 watts/cm² could be obtained.

As in previous studies (1 and 2), the cells were operated at conditions ranging from about 1 amp in the forward direction to where the current becomes nearly constant (light current) in the inverse direction, while the voltage-current characteristic was recorded on an x-y plotter. The light current was used as a measure of the flux incident on the cell.

Results of these measurements taken at several temperatures can be found in references (3) and (4).

Using the distributed diode and resistance model of the cell described in the appendix, it was possible to fit computed current-voltage curves of a cell to the experimental current-voltage curves and to determine the cell parameters.

Using these parameters a second computer program, using the same mathematical model of a cell, was used to determine the optimum number of gridlines at various solar fluxes. This program takes into account the change in optical coverage of the grid, the resistance of the gridlines, and the effect on the surface resistance of the change in distance between the gridlines. The connection strip area (optical coverage) was taken as 10% of the total area, and the area of one gridline (i. e. , the two gridlines on both sides of the connection strip) as 1.38% of the total area. Thus 20 gridlines per cm with a connection strip correspond to an optical coverage of 37.6% of the total area.

Figure 2 gives the computed curves for cell S7 (4), and it can be seen that the optimum efficiency is found at a progressively higher number of gridlines for increasing flux levels. In the range of 24 to 32 W/cm², where the array is expected to operate, it is evident that some gain in efficiency can be obtained by using 20 gridlines/cm instead of 15. The risk involved in relying heavily on these computations is small because the optima are not

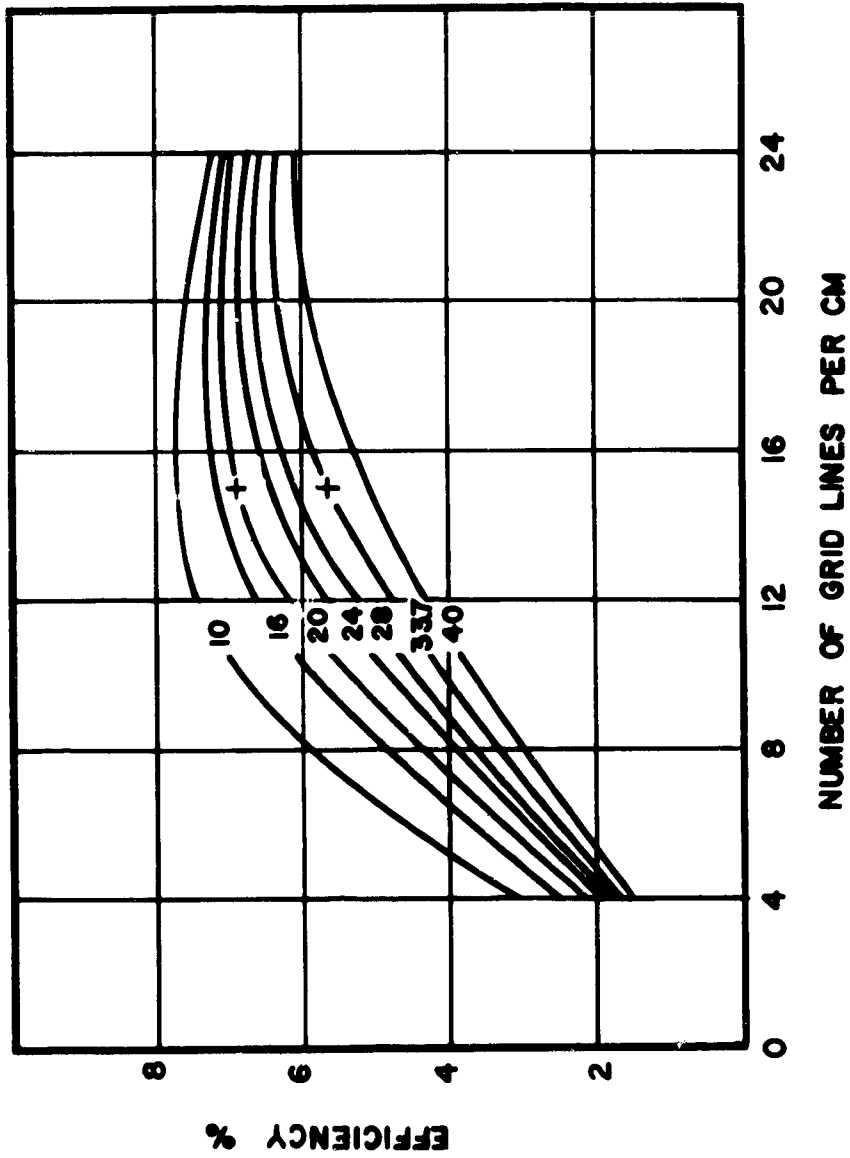


FIG. 2. COMPUTED EFFICIENCY AS A FUNCTION OF NUMBER OF GRID LINES OVER 1 CM AT VARIOUS INPUT FLUNEF (WATTS/CM²). + = MEASURED POINT FOR CELL S7.

sharply defined. It should be noted that curves for low fluxes are not reliable since at high fluxes the open circuit voltage deviates from the assumed exponential relationship used in the mathematical model and in some cases even decreases (probably due to leakage). Consequently, the extreme interpolation from the single measured high flux value to low flux values, yields low open circuit voltages and therefore lower efficiencies than are normally expected.

Fig. 3 shows the theoretical power output at the maximum efficiency condition for an 18 cell array, as a function of the number of gridlines at various solar fluxes. At 33.7 W/cm^2 input, there is a gain of about 8 watts for an 18-cell array with an increase to 20 gridlines/cm from 15 gridlines/cm. These curves do not represent the precise efficiency that can be expected, as individual cells made from the same ingot and produced in the same manner have different efficiencies. However, the trend of efficiency versus the number of gridlines should be the same for most cells.

On the basis of these measurements and extrapolations, it was decided to use cells with 40 gridlines since they would be close to the optimum obtainable output at the expected flux levels. Also, it was evident from these measurements that for the range of cell thickness and diffusion depths tested these variables were not significant (4). Thin cells (with a thickness of .25 mm, i. e., half the thickness of normal cells) were specified since they have better heat transfer characteristics. A diffusion time of 10 minutes at 1090°C , with normal base doping was also specified. Figure 4 depicts the grid configuration.

Unfortunately, due to reassignment of key personnel at the research department of Heliotek, there was a delay in delivery of six months. The cells that were finally delivered proved to be far inferior to cells that had

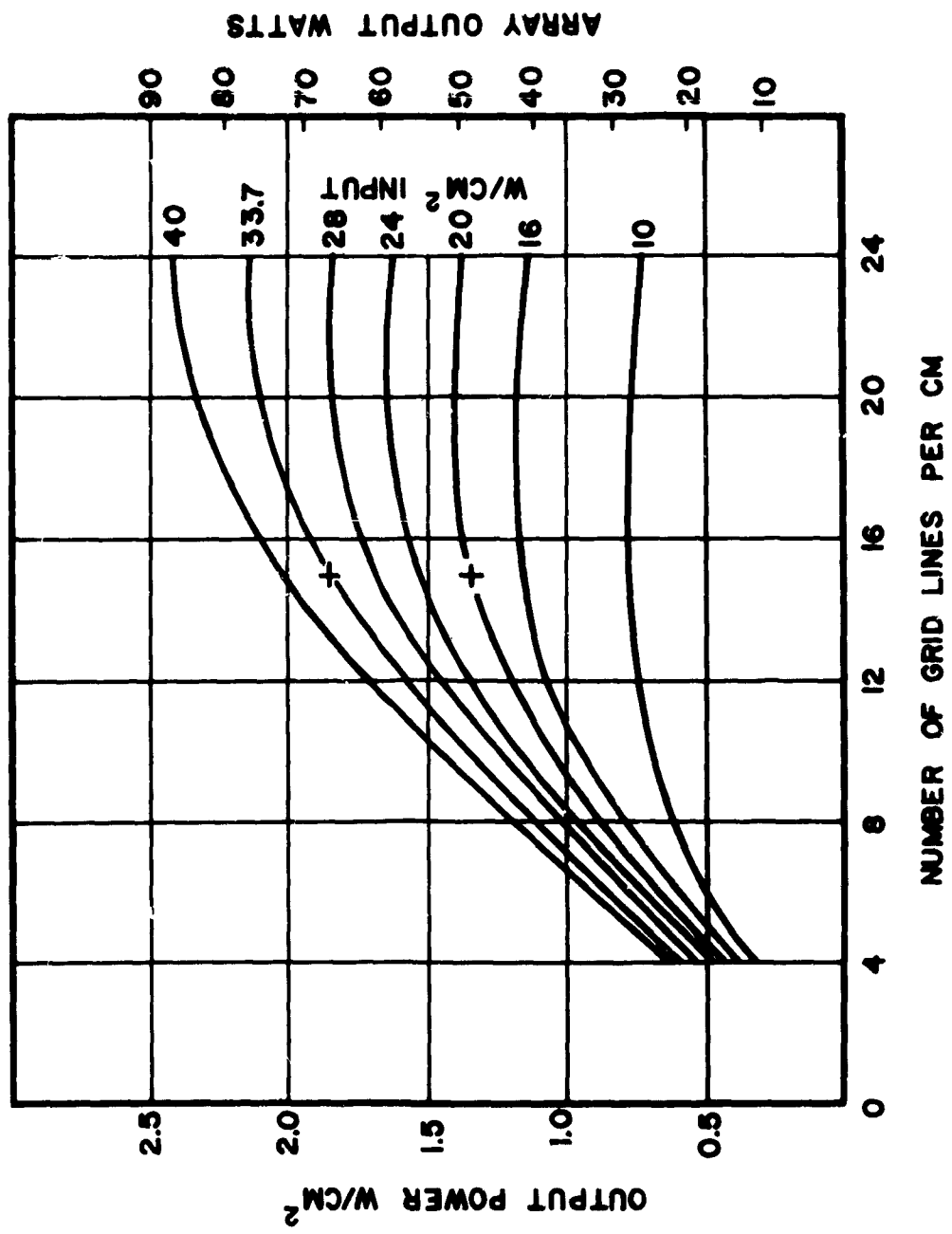
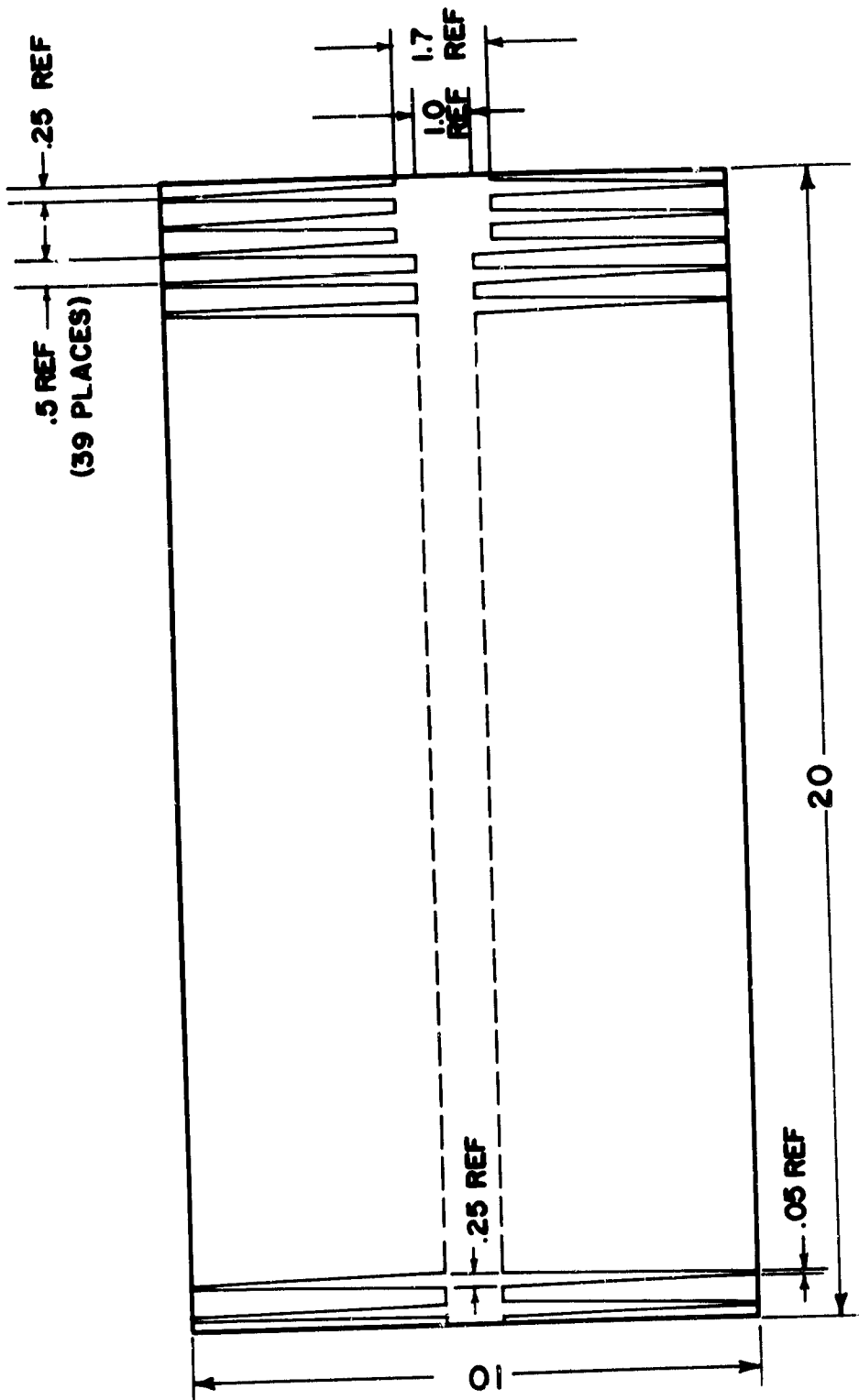


FIG. 3. COMPUTED OUTPUT POWER AS A FUNCTION OF THE NUMBER OF GRID LINES OVER 1 CM, AT VARIOUS INPUT FLUXES



+0 GRIDLINE GRID CONFIGURATION. SIZES IN MM

FIGURE 4. GRID CONFIGURATION

previously been fabricated by the same company.

Due to the difficulty of specifying operating characteristics of experimental cells and because of the late delivery date, it was not possible to refuse acceptance. In view of the reluctance of Heliotek to furnish additional experimental cells, no further work was done on cell optimization.

2. Cell Performance and Conclusions

Out of the 50 cells delivered, 30 were soldered on copper heatsinks as shown in Figure 5 (the heatsinks are described in section C2. The cells were individually measured by mounting the heatsink in a water-cooled clamp in front of a 2 x 2 cm flux distributor which was positioned at the focal point of the solar furnace. The temperature of the heatsink was measured by a thermocouple mounted in a hole in one of the pins. A small cell, biased with an external DC supply, was mounted on the clamp and was used for measuring the incident flux.

Since the 40 gridline cells (SS series) provide about 7% more optical coverage than the 30 gridlines cells (S series), a 7% lower light current output could be expected. Table I gives the light current output per watt of input (I_L/W_i) along with the maximum efficiency of 23 cells. For comparison purposes, I_L/W_i data is also given as a percentage of that obtained from S8. Cell S8 is representative of the S series cells as their light current output did not deviate more than 7.3% from the highest to the lowest value. (Reference (4), Table I, page 7)

The efficiency measurements were taken to weed out the poorest cells and therefore the temperature and flux were not controlled. This makes exact efficiency comparison difficult. All the same, it can be observed that the light current output has little bearing on the efficiency.

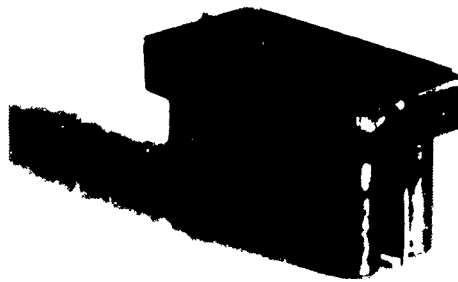


FIGURE 5. CELL AND HEATSINK

TABLE I

Cell	I_L/W_i A/W	I_L/W_i % of S8	Maximum Efficiency %	Flux W/cm ²	T °C
<u>SS</u>					
16	.187	91	3.78	29.2	41
20	.185	90	4.80	29.8	58
25	.178	86	4.64	29.2	63
23	.178	86	5.17	29.7	77
22	.177	86	4.50	29.8	66
10	.176	85	5.37	28.7	50
14	.176	85	4.79	28.8	40
19	.175	85	4.93	28.8	43.5
13	.170	83	5.34	29.2	57
28	.166	81	5.42	28.3	41
12	.161	78	6.46	28.0	41
17	.161	78	5.34	28.8	45
30	.161	78	4.80	28.1	--
5	.159	77	4.47	29.8	41
11	.159	77	4.46	29.2	48
27	.159	77	5.40	29.0	47
7	.153	77	4.34	28.4	60
31	.152	74	5.10	28.7	43
32	.151	73	4.16	29.5	43
8	.147	71	4.00	28.2	--
26	.147	71	4.00	29.8	45
9	.138	67	4.62	28.2	49
6	.132	64	4.74	28.2	63

33-36 were mounted but not measured. Cells with numbers below 30 not appearing in this table were discarded for breaks or poor grids.

The best cell was SS12 which had an efficiency of 6.46%, yet the light current was only 78% of S8, which is lower than ten other cells.

Although it is hard to explain the enormous spread in light current output, the low efficiencies were at least in part caused by poor plating.

The following was evident from a visual check:

Most cells were cut so that the center strip was off center with a deviation of up to 1 mm.

On many cells, gridlines did not have sharp outlines and were poorly tinned.

On some cells the gridlines were not continuous.

Many cells had blobs of plating on the silicon surface.

If cells can be produced which have the characteristics shown in Figure 3, then using 18 cells with 20 gridlines/cm at a solar flux of 28 watts/cm² and at an operating temperature of 90°C, nearly 70 watts of electrical power will be produced. The maximum power point of each cell is about 0.4 volts, thus wiring the 18 cells in series will result in a maximum power point of about 7.2 volts. This voltage is well suited for the charging of a nominal 6 V storage battery. Since the 20 gridline cells actually obtained for use in the breadboard array had considerably lower efficiencies than predicted, the output of the array will also be considerably lower than expected.

C. COOLING SYSTEM

1. Introduction

The solar energy absorbed by the cells will be dissipated in four ways: direct electrical conversion, long wave radiation, convection to the ambient air and forced convection to the water. The cell efficiency is on the order

of 5% so that most of the energy must be dissipated in the form of thermal energy. Because the design of the cell cooling system and solar concentrator proceeded simultaneously with the cell investigation, it was necessary to assume a specific value of the solar input. A total solar input of 1 KW (27.8 watts/cm² on an 18 cell array) was used in the design and performance testing of these systems.

For cell S7, a preliminary curve of cell efficiency versus temperature was extracted from Figure 1 of Reference (3) at a solar radiation of 28W/cm² and is shown in Figure 6. At a cell temperature of about 90°C, the cell efficiency is about 0.6% less than at 66°C. At a nominal power level of 50 watts, this decrease in efficiency results in a decrease in power output for the array of about 6 watts. With a specified maximum ambient air temperature of 49°C, operating the cells at 66°C results in a temperature potential of only 17°C within which the thermal energy must be dissipated to the atmosphere. This potential was found not sufficient for cooling. At a cell operating temperature of 93°C, the 44°C potential was found sufficient for cooling and was used as the preliminary design temperature. Higher cell temperatures have not been considered since no experimental measurements have been made above 93°C.

Both boiling with forced or natural circulation and forced convection with a circulating fluid were considered for cell cooling. After considering both possibilities, forced convection was chosen, with water as the cooling medium.

The main disadvantage of a natural circulation system is that the equipment for dissipating the energy to the atmosphere would have to be located above the cells. Also, in any boiling system, the cells would always operate near the fluid boiling point, even if the ambient temperature was

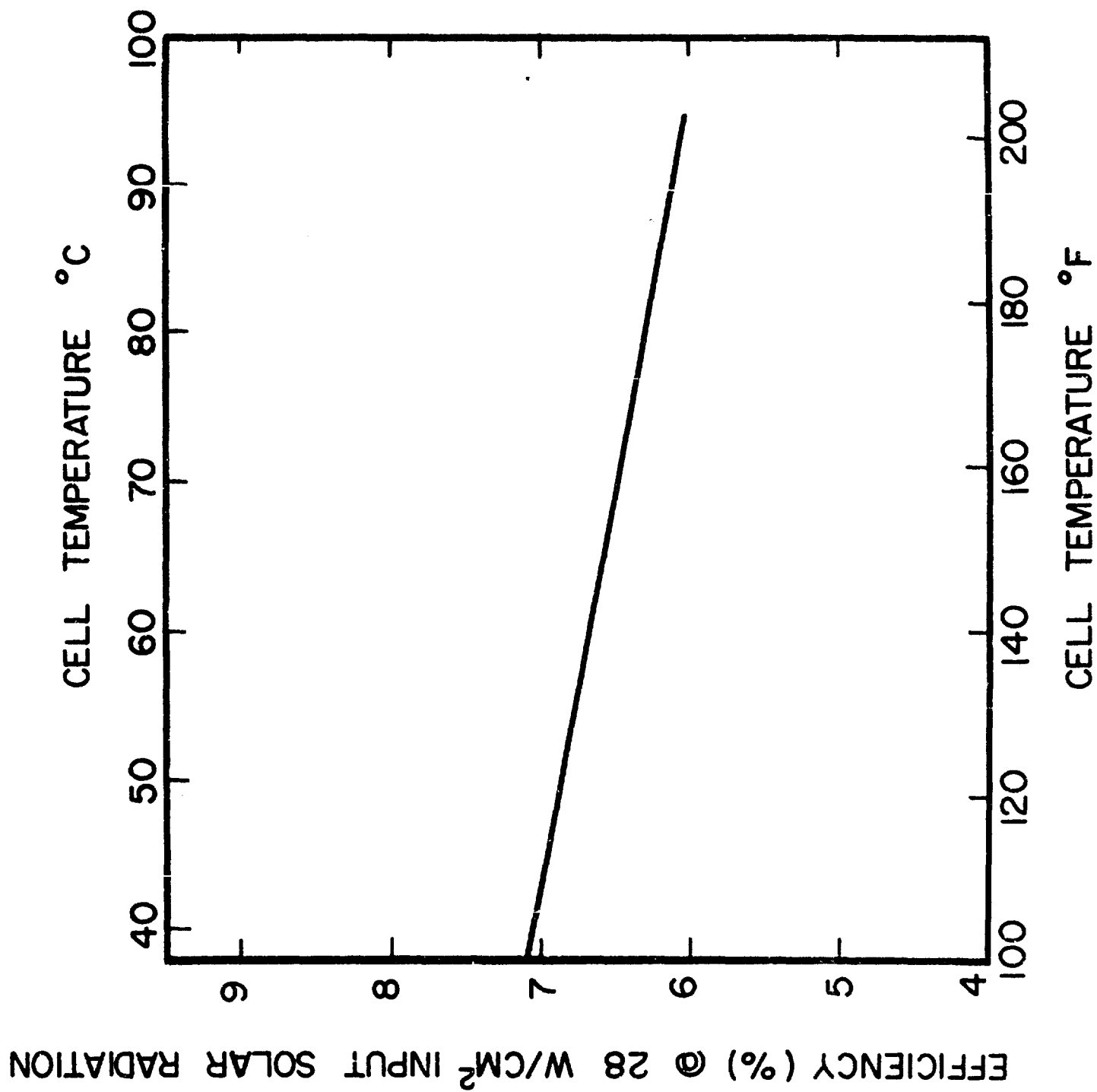


FIGURE 6. TYPICAL CELL EFFICIENCY VS. TEMPERATURE

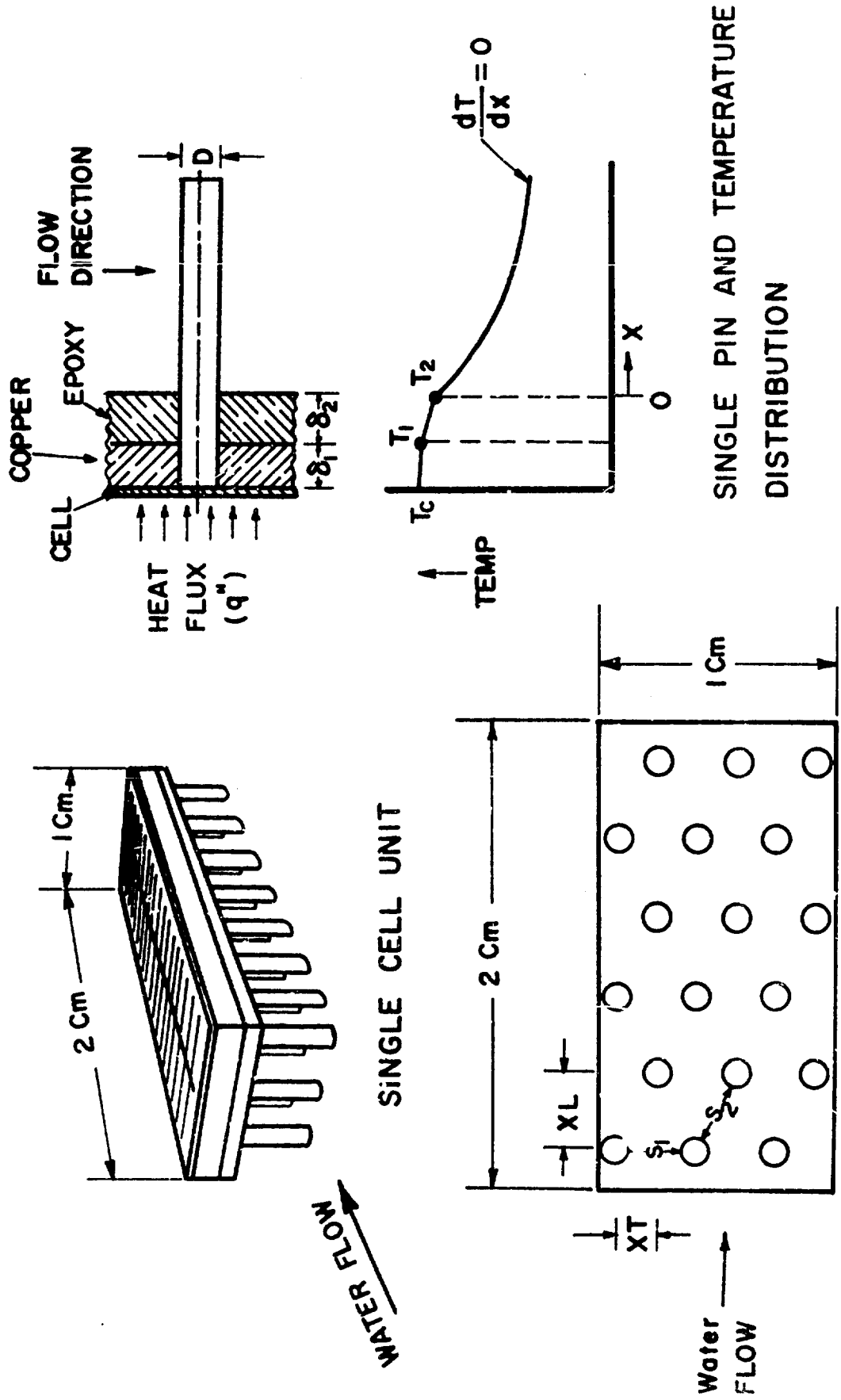
considerably below the design temperature of 49°C. This high operating temperature would result in an unnecessary decrease in efficiency.

2. Cell Cooling System Design and Performance

For the forced circulation system without boiling, an analysis was made for water flowing over a flat plate located behind the cells. The water flow rate necessary to transfer the thermal energy from the cells with a reasonable temperature difference was calculated as well as the minimum work required to pump the water. These calculations showed that for a flat plate 6 cm long in the flow direction, the pump power required to circulate the water with an ideal pump and motor would exceed 5 watts.

To increase the heat transfer from the cells while maintaining a reasonable pump power requirement, it was decided that some type of pinned surface should be extended into the water stream. A theoretical analysis of the pinned heat transfer surface shown in Figures 5 and 7 showed this to be a reasonable solution to the cell cooling problem. In this system, copper pins are soldered into holes in a 1 cm by 2 cm copper plate, and the cell is soldered to the front of the plate.

Since the temperature difference between the cells and the atmosphere is small, the energy dissipation by radiation and natural convection will also be small. Therefore, it was assumed that all the energy absorbed by the cells is dissipated to the circulating water. It was also assumed that the base region between the pins is completely ineffective as a heat transfer surface. Consequently, all the energy transfer occurs between the pins and the cooling water. The temperature difference between the underside of the cells (T_c) and the cooling water (T_{∞}) can then be found by assuming one dimensional conduction from the back of the cells to the pin base and



$S_{min} = \text{Minimum of } S_1 \text{ Or } S_2$

TYPICAL STAGGERED PIN GEOMETRY

FIGURE 7. CELL HEAT SINK CONFIGURATION

then using standard extended surface heat transfer calculations (3). This analysis results in

$$T_c - T_\infty = \frac{4q'' A_c \delta_2}{Nk_p \pi D^2} \left[1 + \frac{1}{\delta_2 m \tanh mL} + \frac{N \delta_1 D^2 \pi}{4 \delta_2 A} \right] \quad (1)$$

where the dimensions δ_1 , δ_2 and D are shown in Figure 7 and

- q'' = absorbed solar radiation
- A = total cell area
- N = number of pins in the array
- $m = 4h/k_p D^{1/2}$
- k_p = thermal conductivity of the pins
- h = heat transfer coefficient

The heat transfer coefficient (h) was determined from an empirical correlation by Grimison (5):

$$Nu = 1.11 C (Re_{\max})^n (Pr)^{1/2} \quad (2)$$

where

- Nu = Nusselt Number
- Re = Reynolds Number
- Pr = Prandtl Number

C and n = Empirical Constants listed in reference 5.

and all fluid properties are evaluated at the average film temperature. The maximum Reynolds number is determined using the water velocity through the minimum pin spacing (S_{\min}) as shown in Figure 7. (For inline pins $S_{\min} = S_1$).

With the cell temperature specified at 93°C, the optimum cooling system design (aside from cost considerations) will be the one with the minimum

auxiliary power requirements. Actually, a system optimization technique should be used with the cell temperature (and thus the cell efficiency) as one of the variables. However, the complexity is greatly increased while the data on temperature dependence of efficiency are of a preliminary nature.

For a fixed water flow rate, pin diameter, and pin spacing, there is a particular pin length at which the temperature difference $T_c - T_\infty$ is a minimum. This minimum can be found by differentiating Equation 1 with respect to the pin length and setting it equal to zero. This operation results in a transcendental equation for the pin length in terms of m (which is also a function of L since the heat transfer coefficient is a function of L for a fixed water flow rate) and the empirical exponent n in Equation 2.

$$\frac{2}{n} - 1 = (\sinh mL) (\cosh mL) / mL \quad (3)$$

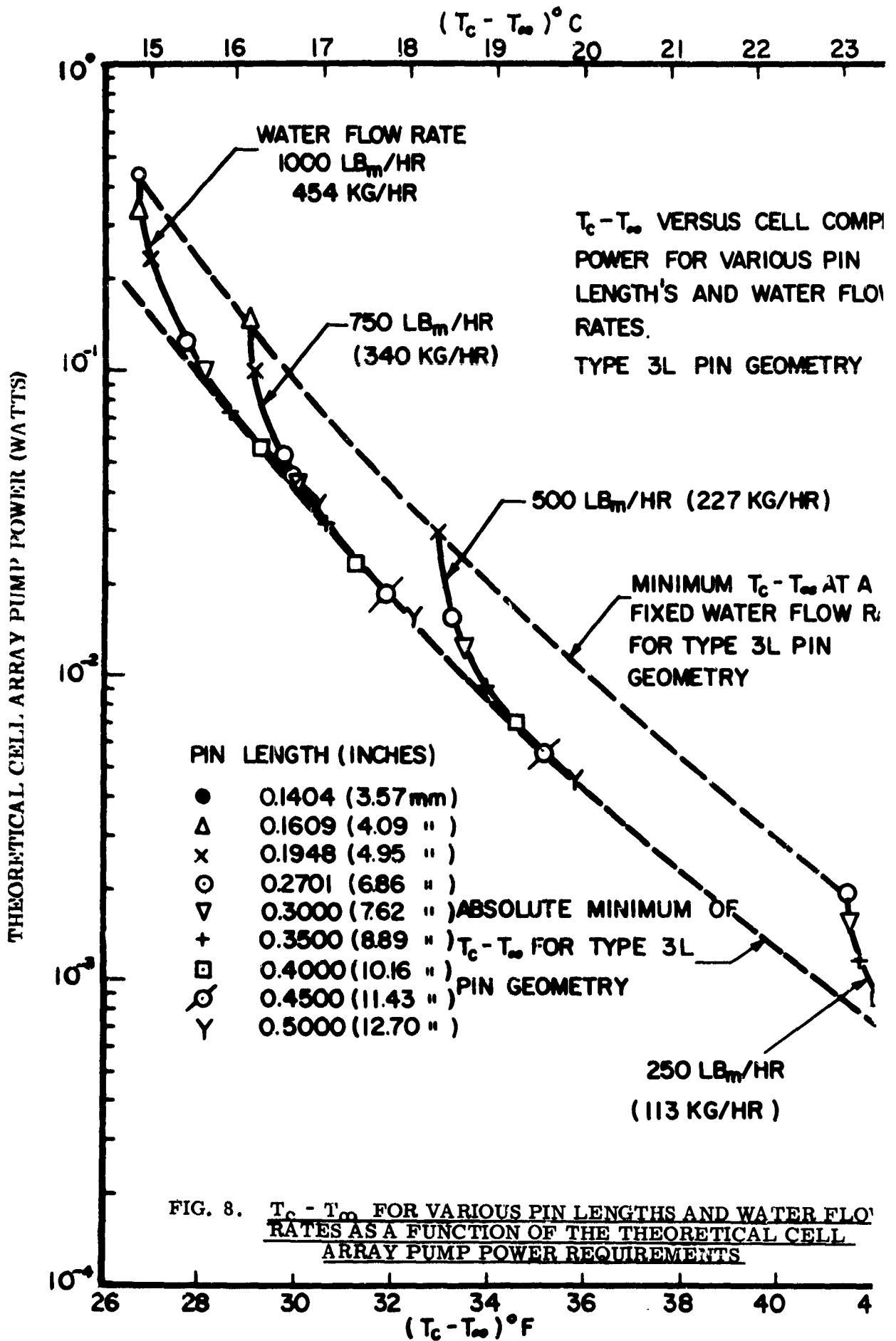
The pin length obtained from Equation 3 does not represent the best design condition since the energy required to pump the cooling water may be excessive. The cell array pump power requirement for several different pin spacings and pin diameters was calculated from an empirical correlation by Jakob (5). The theoretical pump power and the minimum cell-water temperature difference for 20 different pin geometries were investigated and the seven most promising designs are shown in Figure 8 of reference (3). After comparing the temperature difference ($T_c - T_\infty$) and the cell array pump power for the seven designs, two pin geometries were selected for further analysis and are referred to as types 3L and 1S. The pins for type 3L design are 0.318 cm in diameter and spaced in an inline pattern on 0.516 cm centers. The pins for type 1S design are 0.159 cm in diameter and are spaced in a staggered pattern on 0.318 cm centers.

During prototype construction of type 1S heat sinks, it was found that due to the large number of pins required for each cell (25), construction was very difficult. Type 3L required only 8 pins on each cell and was reasonably easy to build. Consequently, type 3L was selected as the design for the breadboard model.

For a given water flow rate, pin geometry and absorbed solar energy, an increase in the pin length will increase the value of $(T_c - T_\infty)$ but will decrease the pump power requirement (P). For type 3L pin geometry, $T_c - T_\infty$ and P are plotted in Figure 8 for various pin lengths, for four different water flow rates and for an absorbed solar energy of 1 Kw. An absolute minimum value of the temperature difference $(T_c - T_\infty)$ for a particular pump power requirement can be found by taking the envelope curve as shown in the figure. For an absolute minimum of $(T_c - T_\infty)$ between 15°C and 22°C, the theoretical cell array pump power decreases from 10^{-1} to 10^{-3} watts. If the water flow rate is 227 kg/hr and the pin length is 0.76 cm, the theoretical pump power for the cell array will be about 0.01 watt. This combination of pin length and water flow rate was chosen as the design condition and results in a value of $(T_c - T_\infty)$ of 19°C.

The performance of the cell cooling system was established by an experimental program utilizing the test equipment described in reference (6). This experiment used an electrically heated simulation of the cell cooling system with type 3L pin configuration.

The electrical heaters were constructed of nichrome ribbon wound over a sheet of mica. Considerable difficulty was encountered in building an electrical heater which would deliver the required amount of power without burning out. In order to obtain heat transfer data at the design solar input power level of 1 Kw, it was necessary to take measurements at low



power levels and extrapolate to the design condition. Measurements of the temperature difference between the simulated underside of the cell and the cooling water ($T_c - T_\infty$) were taken at 250, 500 and 850 watts. The temperature difference exhibited a linear relationship with input power and was extrapolated to 1 Kw. This linear relationship was expected since the analytical prediction (Equation 1) exhibits a linear variation.

For a simulated solar input of 1 Kw, the experimental data for three pin lengths is shown in Figure 9 along with the analytical prediction (extracted from Figure 8). The agreement between measured and predicted values is good over the range of test conditions since the maximum difference, at a pin length of 1.27 cm and a water flow rate of 300 Kg/hr, is only 1°C.

The water pumping power was determined from measured water flow rates and pressure drops across the simulated cell cooling system. Because of very small powers involved (10^{-3} to 5×10^{-2} watts), they were difficult to measure accurately, however, for the range of experimental conditions the pumping power was within $\pm 50\%$ of the predicted values shown on Figure 8.

3. Air Heat Exchanger

The air heat exchanger is required to transfer 1 Kw of thermal energy from the cooling water to still air at a design ambient temperature of 49°C. The original concept was to use a forced convection finned tube commercially available heat exchanger with a small fan and motor to circulate air over the coils. After an extensive but fruitless search for an efficient fan and motor combination capable of moving the required quantity of air across the coils with an electrical power consumption of less than 5 watts, it was

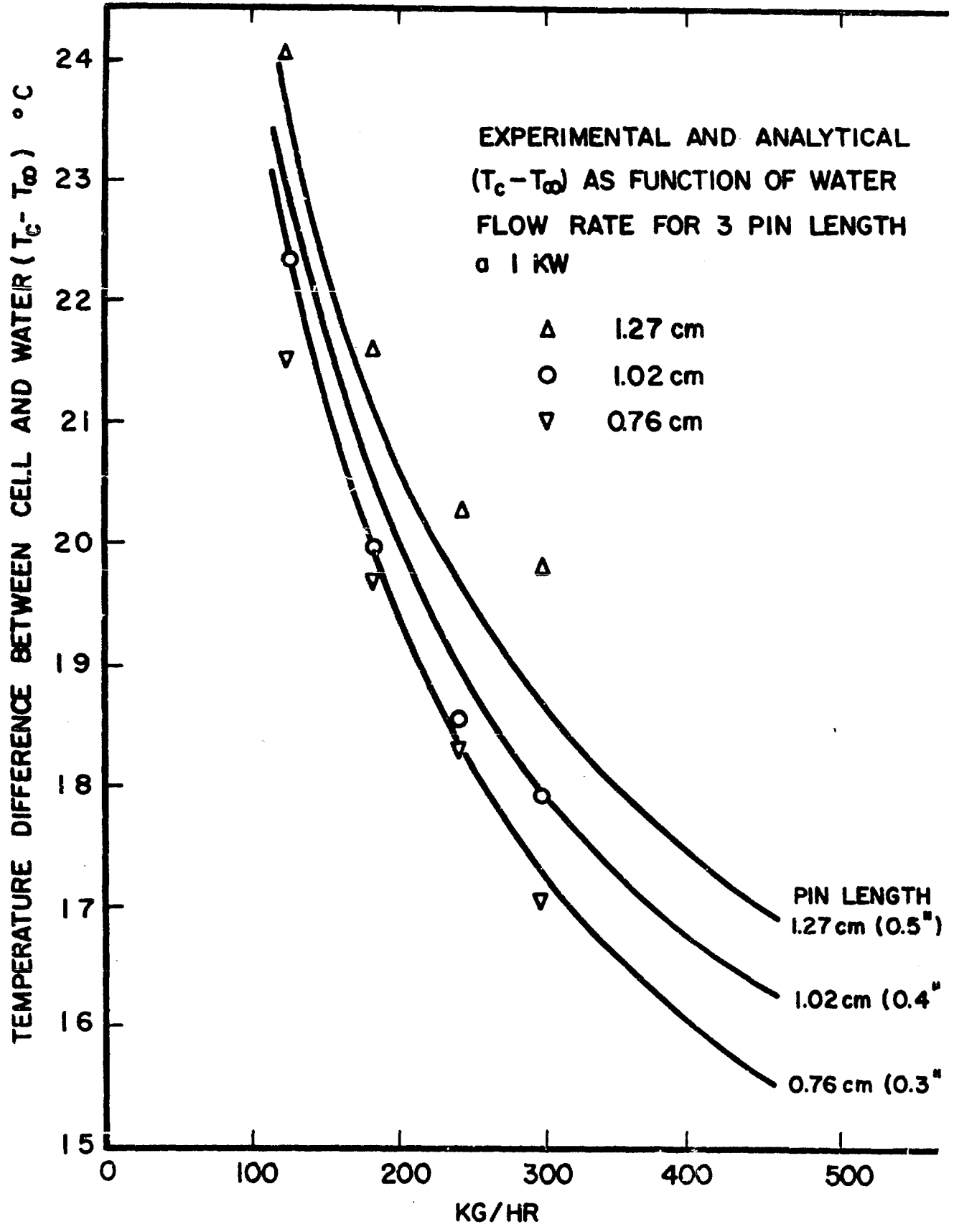


FIGURE 9. EXPERIMENTAL ($T_c - T_w$) VS. WATER FLOW RATE FOR 3 PIN LENGTHS

decided to eliminate the fan and motor and use a free convection heat exchanger.

The water flowing through the cell array will be heated about 4°C with a solar input of 1 Kw (28 watts/cm²) and a water flow rate of 227 kg/hr. Thus, with an average cell temperature of 93°C and $(T_c - T_\infty)$ equal to 19°C, the water temperature will be 72°C at the inlet and 76°C at the outlet. If no thermal losses occur in the tubing between the cell array and the air-water heat exchanger (any thermal losses are of course desirable), the water inlet temperature to the heat exchanger will also be 76°C. Using the design ambient temperature of 49°C, an average temperature difference of 25°C is available for dissipating the thermal energy from the water to the atmosphere. A free convection heat exchanger with a 18.5 cm high chimney using 6 fins per inch on 13 tubes with an overall size of 61cm by 61 cm is sufficient to dissipate 1 Kw of thermal energy to the atmosphere at these temperatures. If the heat exchanger is ducted so that any available wind assists the free convection, and if the ambient temperature is below 49°C, the cells will operate at a lower temperature and thus a higher efficiency.

The air heat exchanger was designed using finned tube free convection heat transfer correlations supplied by the manufacturer (Rempe Co., Chicago, Ill.). However, due to the large uncertainty in predicting free convection heat transfer coefficients, it was found that the design did not meet the required performance.

The performance was increased by adding a chimney to the heat exchanger which increases the static pressure head and thus the air velocity and heat transfer coefficient. Figure 10 presents the experimental data on

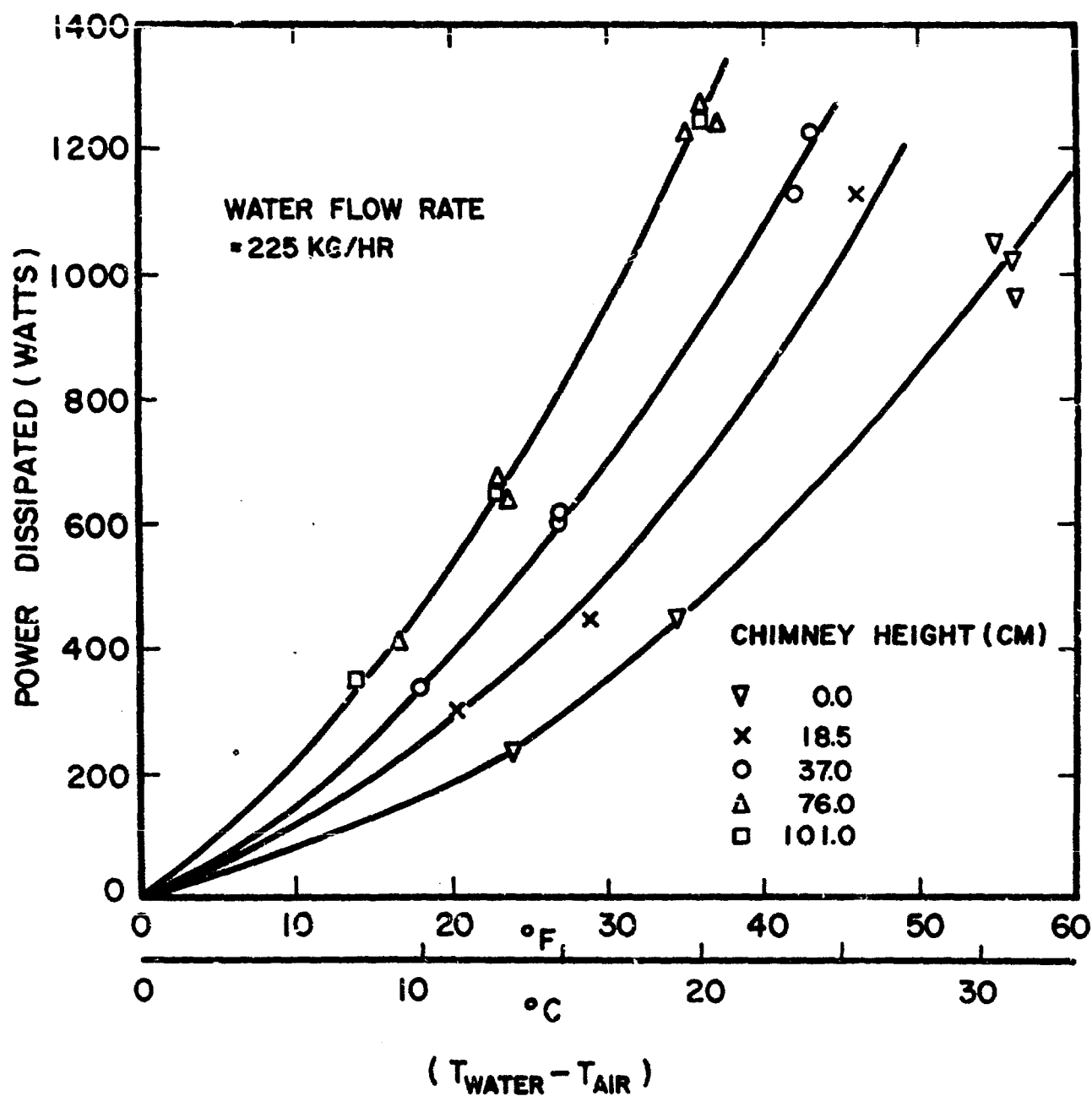


FIGURE 10. AIR HEAT EXCHANGER PERFORMANCE

the heat exchanger operating in still air with 5 different chimney heights between 0 and 101 cm. The data was taken at a water flow rate of 225 Kg/hr, but no significant changes were found when the flow rate was decreased to 112 Kg/hr. This independence of performance on the water flow rate was expected since the resistance to heat transfer between the water and the tubes is very much smaller than the resistance between the fins and the air.

In order to simulate the original design conditions of 1 Kw thermal energy dissipation at an average temperature difference of 25°C, a chimney height of 18.5 cm was selected for the breadboard model.

With the particular heat exchanger used, the average water temperature and consequently the average cell temperature could have been reduced by 8°C by using a 76 cm chimney. Alternatively, a smaller heat exchanger with a chimney could have been used at the design conditions.

An additional advantage of large chimney heights is that the chimney shades the heat exchanger from direct solar radiation. With a .37 square meter heat exchanger frontal area, the direct solar input could exceed 1/3 of the required dissipation rate which would result in an increase in the cell operating temperature. If the chimney were painted black, an additional increase in the performance would result due to heating of the air above the heat exchanger. The increased air temperature above the heat exchanger would further increase the available static pressure head and consequently the air velocity across the heat exchanger.

4. Pump and Motor

The specification of a closed loop cooling system requires the use of a pump and motor to circulate the cooling fluid. A natural circulation cooling system without a pump and motor was not considered in detail since the air-water heat exchanger used for energy rejection must be located above the cells. This places restrictions on the system configuration which were considered too severe.

Inquiries were made of about 15 manufacturers for a pumping system with the following specifications:

1. Operation on 6 ± 1.5 V
2. Delivery of 225 Kg/hr of water
3. Head ranging from zero to 25 cm of water
4. Power consumption not to exceed 5 watts. (This specifies a 6% efficiency at 50 cm head.)

None of the manufacturers could meet these specifications with available equipment. Consequently, it was decided to modify commercially available equipment to meet the specifications.

The pump finally chosen is a Peters and Russell positive displacement diaphragm pump (Model 4960). Specified commercial use is light, or intermittent duty. Commercial performance is .32 liter/sec. discharge with a maximum suction lift of 1.5 m. and a maximum discharge head of 1 m. With the 12 V motor supplied with this system, the electrical consumption is approximately 50 watts.

The pump was modified to meet the requirements of 225 Kg/hr of water (approx. 1/2 gal/min) at a total discharge head of 25 cm of H_2O . The modifications include the removal of the existing D.C. motor drive, the

installation of new bearings, the addition of a flywheel for the test program and provision for changing the crankshaft stroke and connecting rod length. The commercial diaphragm, valves and water reservoir were retained.

The procedure for testing the pump was based upon determining power input to the pump shaft by means of a transient speed decay curve for a given pressure drop and crankshaft stroke. From the transient speed decay curves the angular deceleration of the pump shaft was measured. Using this information along with the known moment of inertia and the shaft speed, the shaft power can be calculated. The speeds are chosen to give a specified flow rate for a given crankshaft stroke.

The crankshaft strokes tested ranged from 1.59 mm to 7.95 mm. The commercial unit is supplied with a 4.76 mm (3/16") stroke. Preliminary tests showed that for flow rates below 340 Kg/hr, the 7.95 mm and 6.36 mm strokes are unsatisfactory due to violent pulsations in the water flow, which shake the entire system. The 0.79 mm stroke is also eliminated because it requires excessively high rotative speeds and power consumption to deliver the desired flow rate.

The final test results are plotted on Figures 11, 12 and 13. These results include the 4.76 mm, 3.18 mm and 1.59 mm stroke crankshaft data with emphasis on the 4.76 mm and 3.18 mm strokes.

An important feature of this pump when used for flow rates of 225 Kg/hr or less is the linear variation of water flow rate versus pump speed. Figure 11 shows this characteristic. Above 225 Kg/hr, the flow rate is decreased by increased heads.

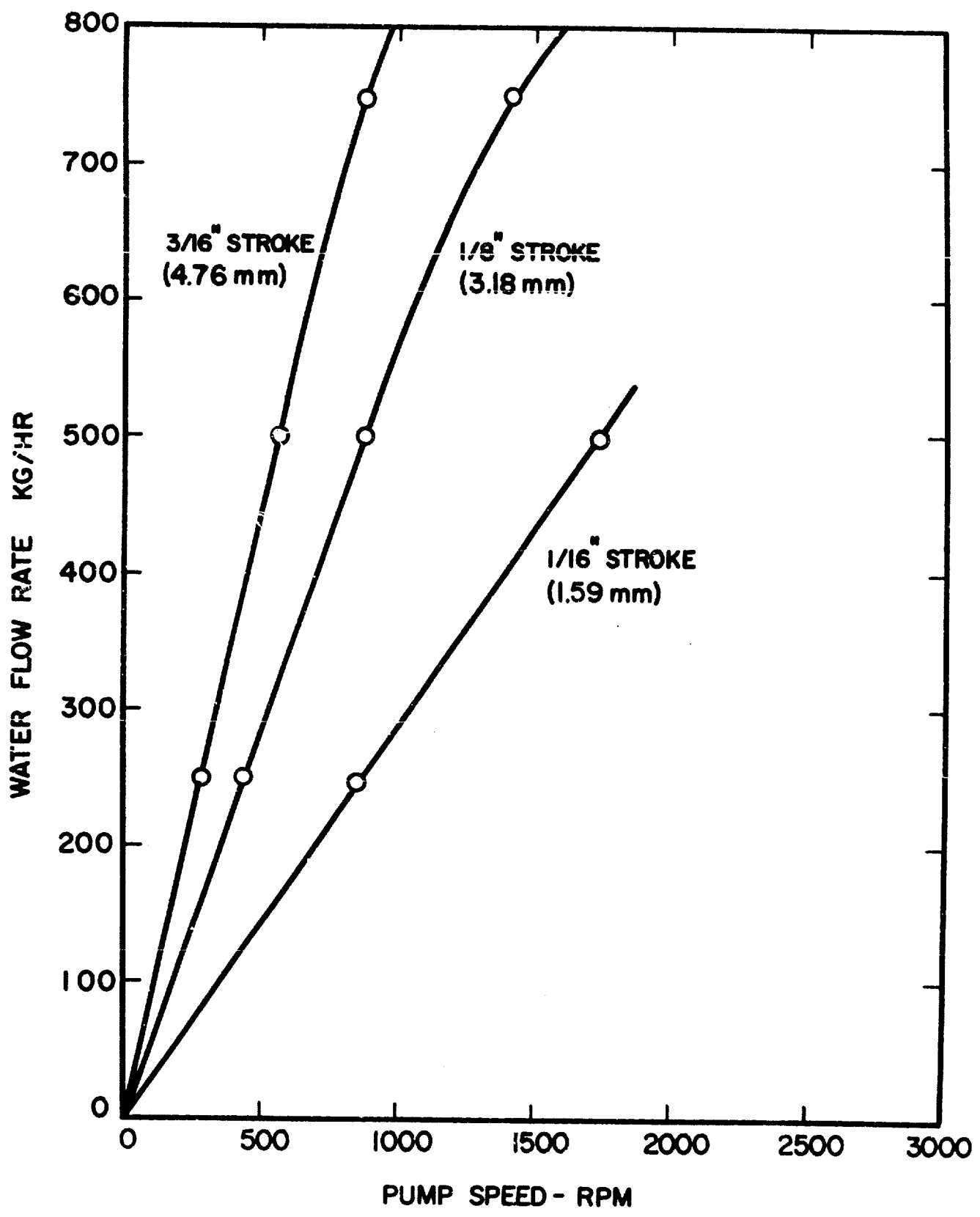


FIGURE 11. PUMP FLOW RATE VS. RPM

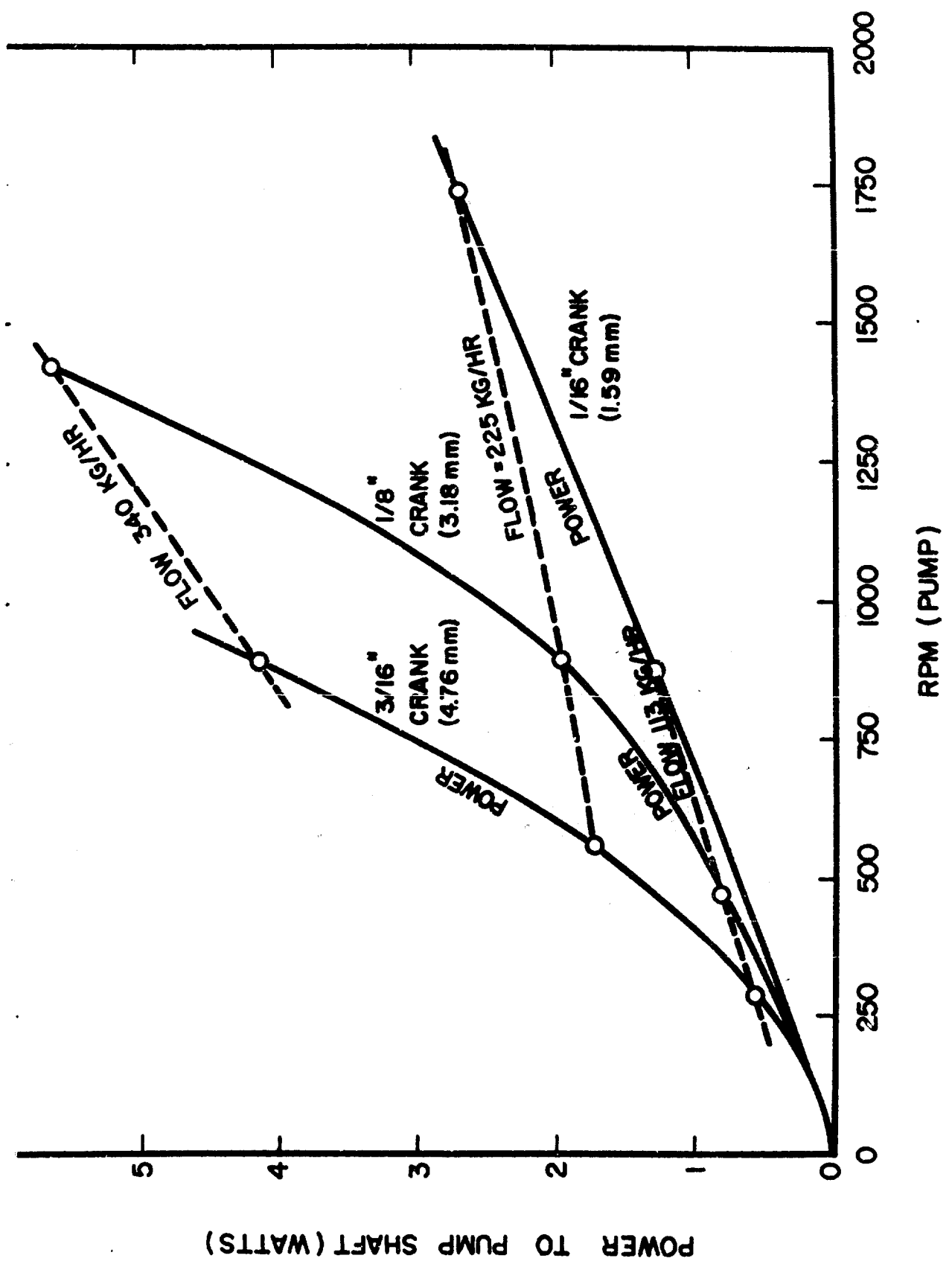
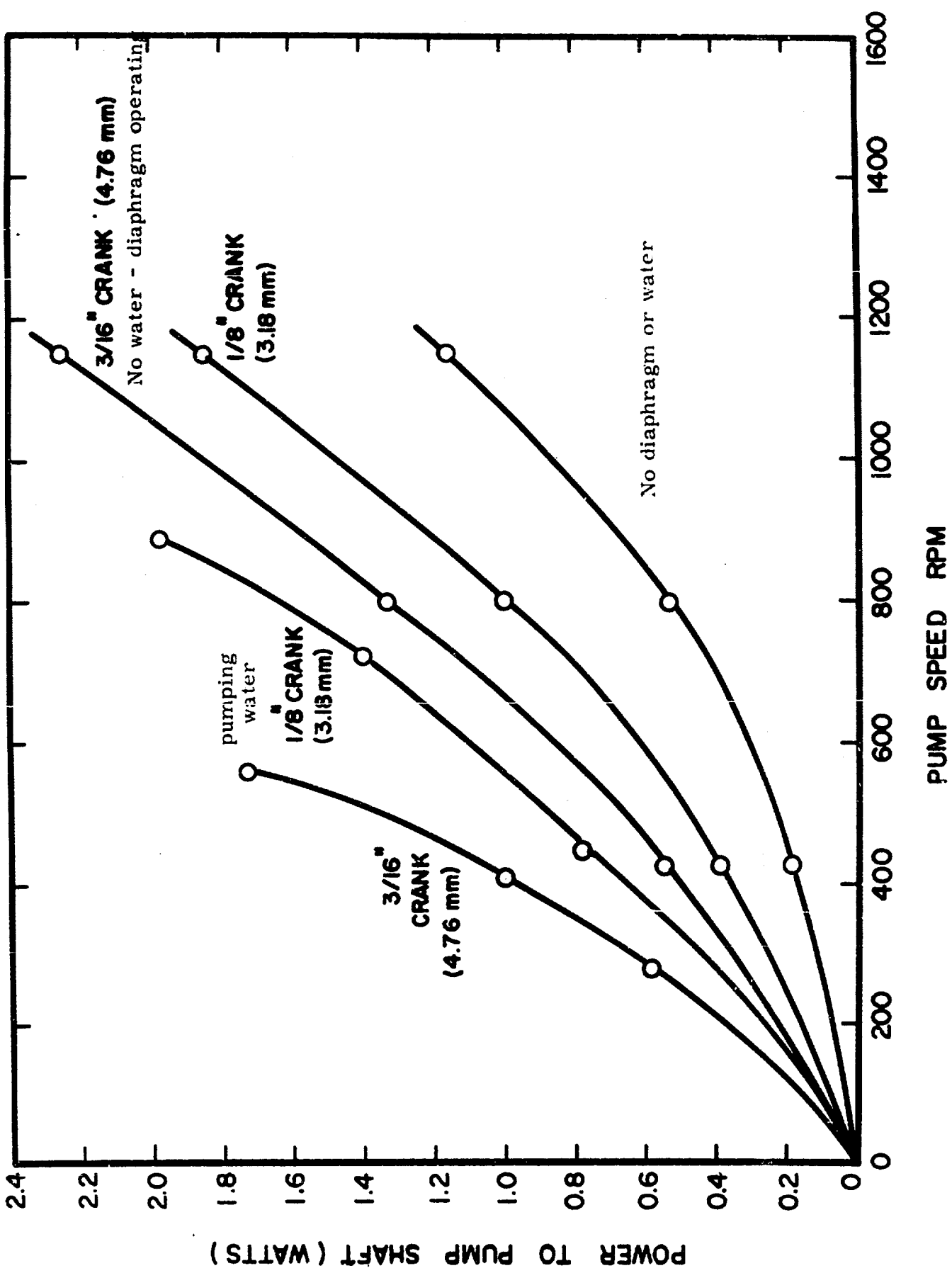


FIGURE 12. PUMP POWER VS. RPM



ar
st
st
in
po
is
4.
be
ar
ph
th
br
du
cc
(M
be
m
of
po
th
tes

The data for power input to the pump shaft versus the pump speed are displayed in Figure 12. Superimposed on this graph are lines of constant flow rate. This figure shows that for a given flow rate, the stroke crankshaft requires the least amount of power. Decreases in stroke increase the pump speed and power input for a given flow rate.

The relationship between total input power to the pump and the corresponding internal power consumed by the diaphragm, bearings and windage is recorded on Figure 13. For a flow rate of 225/Kg/hr and a stroke of 4.76 mm, 44% of the 1.74 watts input power is consumed by the diaphragm, bearings and windage. Of this 1.74 watts, 16% is absorbed by the bearings and windage. Therefore, it can be concluded that a better designed diaphragm and valves would improve the pump's overall performance.

Since with the original pump diaphragm, a stroke of 4.76 mm produces the maximum flow at a given input power, it was selected to be used in the breadboard system. The design speed was selected as 600 rpm which produces the 225 Kg/hr flow specified by the cell cooling design. At these conditions, the shaft input power is about 1.8 watts.

The motor selected to be used with the pump was a Globe gear motor (Model No. C43A101-18). This motor normally operates at 6 V but has been operated over 9 V during system tests without overheating. The motor will also operate as low as 3.5 V before stalling.

The motor was purchased with a preassembled gearbox with a reduction of 22:1. This particular reduction was selected to match as close as possible the required pump rotational speed when operating at 6 V. Since the gearbox output shaft was smaller than the drive shaft used for pump testing, smaller ball bearings were installed on the pump shaft. This

change has some effect on the pump characteristics, but the pump itself was not tested with the new bearings.

A test was performed on the pump and motor combination in order to determine the overall characteristics. Figure 14 shows the water flow rate and electrical input power as a function of motor voltage for zero head. Tests at 25 cm head resulted in water flow rates only a few percent lower and power consumption only a few percent higher than at zero head. The figure indicates that at 6 V, the flow rate was 182 Kg/hr and the electrical power input was 4 watts. The reduced flow rate was due to the limited selection of gear reductions available with the Globe gear motor. The next available gear reduction was 14.58:1 which would have produced a flow rate of about 270 Kg/hr with a power consumption of over 6 watts. With a gear reduction of about 17.5:1 on this particular motor, the flow rate would be about 225 Kg/hr and the power consumption would be about 5 watts at 6 V.

With the present system, the flow rate and power consumption will be about 225 Kg/hr and 5 watts when the power supply is in normal operation, since the charging voltage will be about 1.5 volts above the nominal battery voltage.

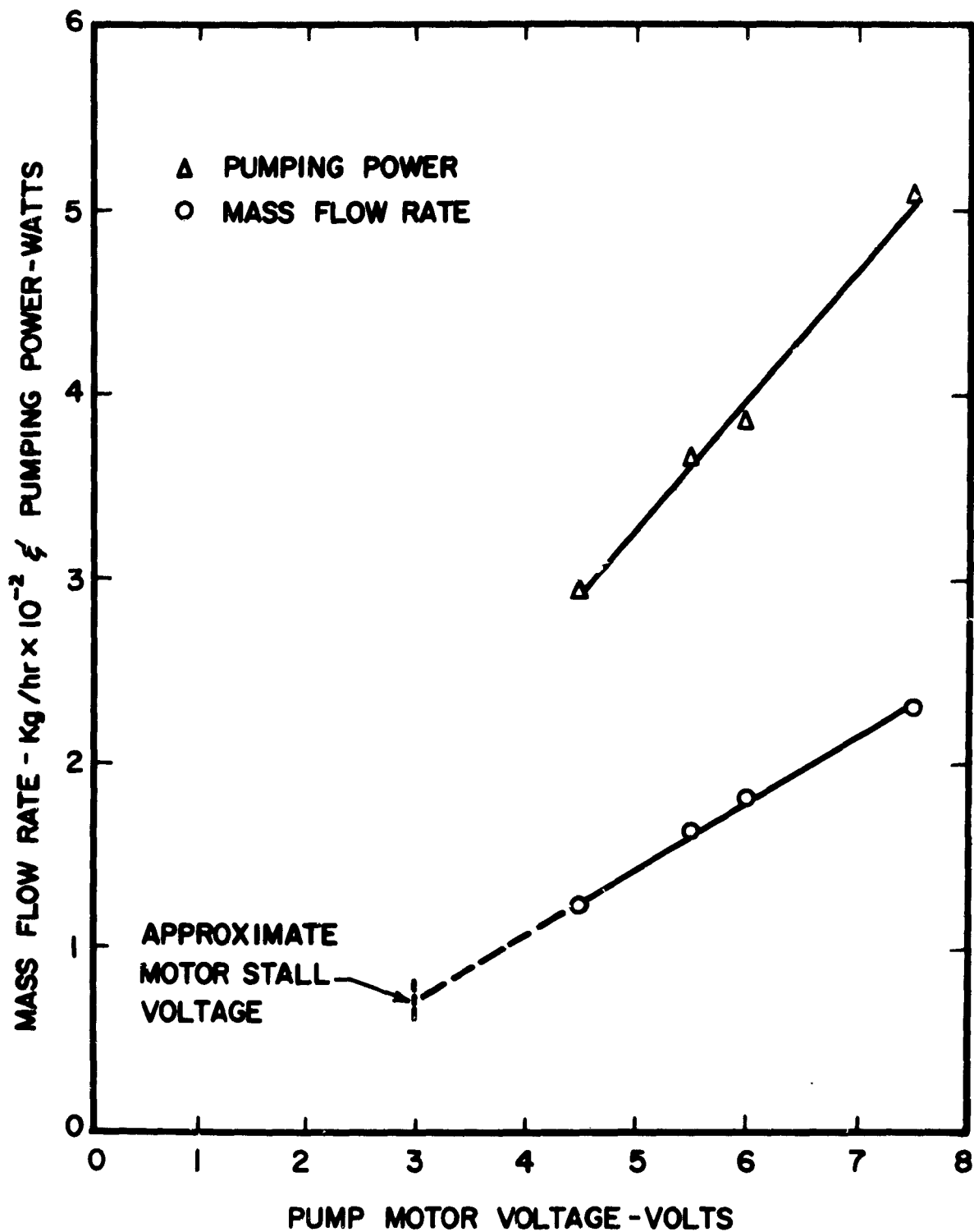


FIGURE 14. PUMP AND MOTOR CHARACTERISTICS AT ZERO HEAD

D. SOLAR REFLECTOR

The breadboard solar concentrator was constructed using 416 individually adjustable mirrors 7.4 cm square. Each mirror was individually mounted on a 1.8 meter diameter epoxy-fiberglass shell approximately parabolic in shape with a 1 meter focal length.

The mirrors were glued at their centers to 7.4 cm square aluminum plates. Each plate had 3 countersunk holes into which 3 flat head machine screws were placed. The screws passed through 1.5 cm long rubber spacers and then through holes in the epoxy shell. With this system, each mirror could be individually adjusted by tightening the nuts on the machine screws.

The alignment of each mirror of the reflector was accomplished by optical means. A small nearly parallel beam of light, generated by a zirconium arc lamp and a condensing lens, was located at the collector focal point and mounted in a swivel. A large mirror was located perpendicular to the collector axis. The light beam was directed to the center of one of the collector mirrors and reflected to the large mirror. When the collector mirror was correctly aligned, the light beam reflected off the large mirror and retraced its path back to the focal spot. Thus adjustment of each mirror's support screws, while observing the spot of light on a mask near the focal plane, enabled each mirror to be correctly oriented. The collector was placed in a horizontal position with the focal axis pointed upward during the alignment operation. The large mirror was positioned above any desired area of the collector and was adjusted perpendicular to the focal axis by a precision level.

Measurements were made of the flux distribution at the focal plane on a clear day when the direct solar radiation was 1.118 Ly/min (0.078 watts/cm²). The flux measured at the center of the array was 369 Ly/min (25.7 watts/cm²) which is a concentration ratio of 313. If the beam radiation had been equal to the design value of 0.090 watts/cm² the flux at the center would have been 29.7 watts/cm².

The flux uniformity over the cell array was not as good as expected. Figure 15 shows the relative flux at various points on the array. The flux at the center of the four corner cells was between 8 and 16 percent lower than at the center of the array. The reason for this nonuniformity is probably due to distortions of the shell when the reflector is not in a horizontal position as it was during mirror alignment. This type of reflector system was not intended to be used in an operational system. The reflector was designed as an attempt to obtain uniform flux with the additional possibility of obtaining lower fluxes with uniform intensity by covering some of the mirrors.

A more uniform flux distribution over the cell array could be obtained by using a paraboloidal surface with a flux distributor (6). It is estimated that this type of reflector could be constructed with a collection efficiency of over 50%. The breadboard collection efficiency based on the measured flux at the center of each cell was about 42%. Thus it appears that reduction of the collector size is possible.

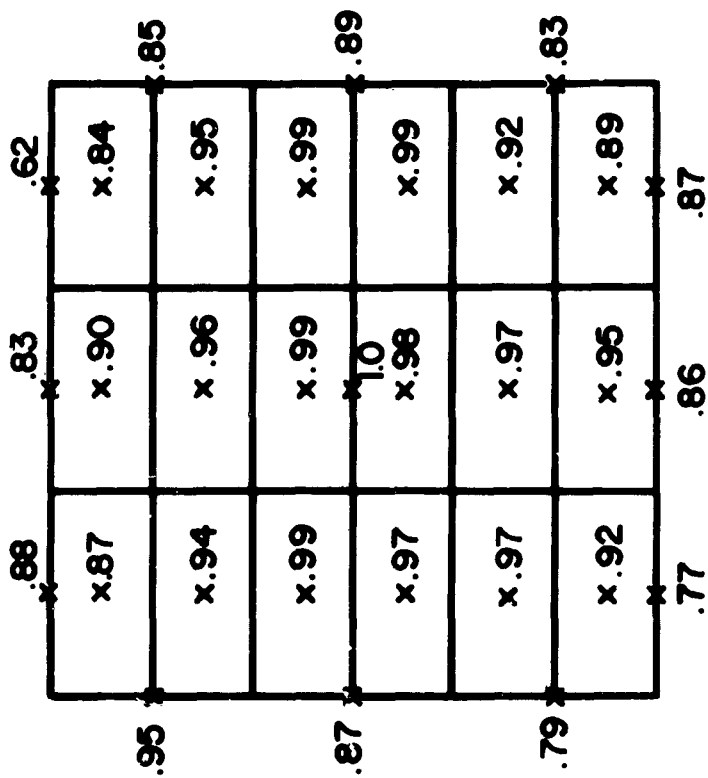


FIGURE 15. FLUX DISTRIBUTION ON CELL ARRAY

E. ELECTRICAL CONTROL SYSTEM

An electrical control system was required with the following characteristics:

1. It should prevent discharge from the battery through the cells when no current is generated by the cell array.
2. The pump motor should start and run as soon as cooling is required. This implies that low voltage conditions of the battery must not endanger the pumping of coolant.
3. The losses in the switching system must be zero in standby condition and low at normal output levels.

A diagram of the switching system is depicted in Figure 16. A sigma 26F relay RL1 is used as a current sensing device. It was rewound with 16 turns of copper strip to obtain a low resistance relay.

A separate switching relay RL2 with two interlocking armatures is used to bypass a rectifier and resistor which initially pass the array current to the battery.

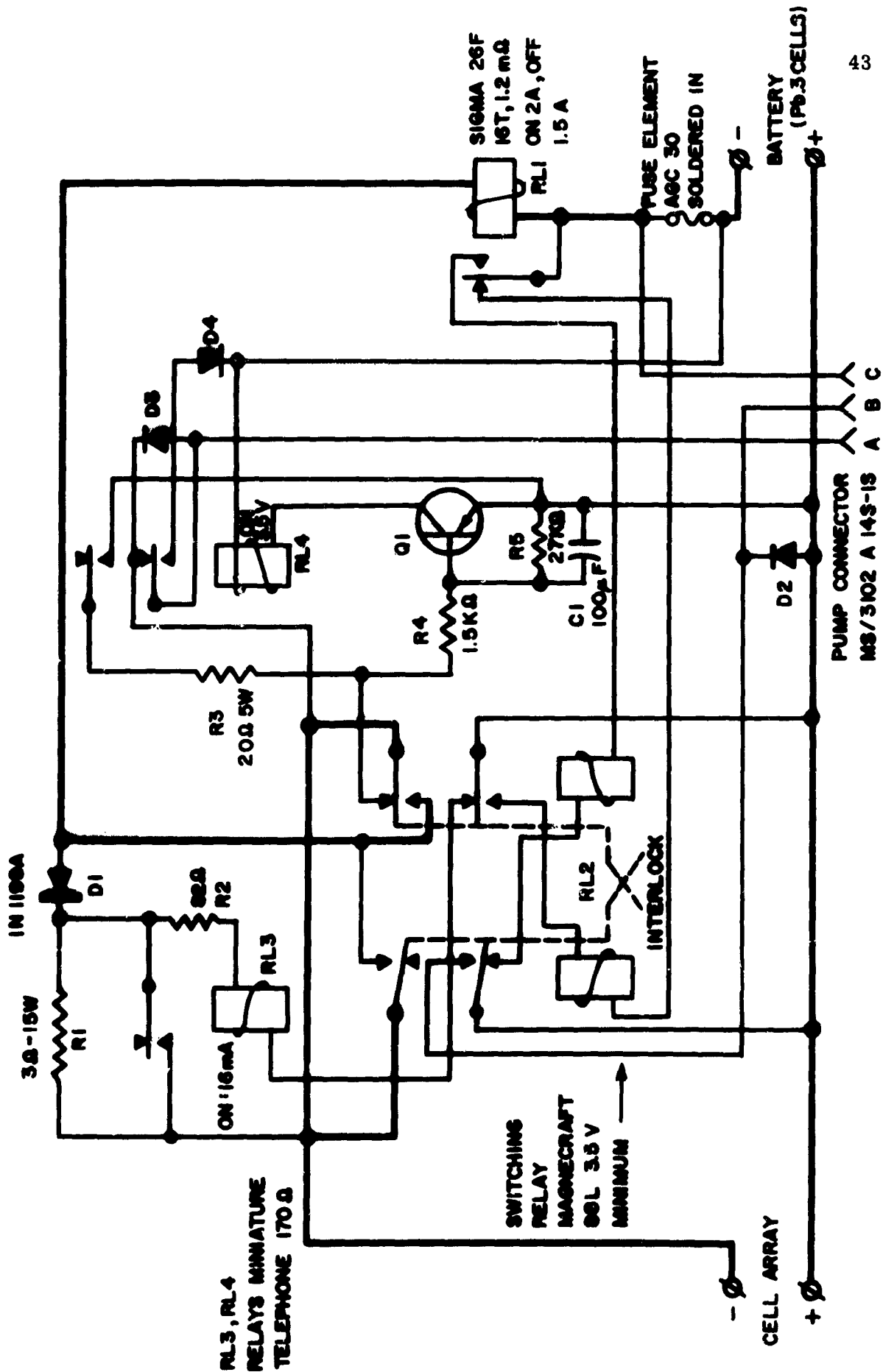
RL2 is self-interrupting, thus draws no standby current and is controlled by the current relay.

The rectifier D1 prevents battery drainage through the cell array when the cell voltage is lower than the battery voltage.

The resistor R1 is provided to insure enough voltage for the coolant pump in case of low battery voltage. When the voltage at the connection between the rectifier and R1 exceeds 4 volts to common, R1 is shorted out by the voltage relay RL3.

RL3 is switched off by RL2 to prevent extra loss when normal conditions prevail.

R1 drastically limits the charging current in case of a "dead" battery, but if the battery has no load and is not irreversibly damaged, it will



RL3, RL4
RELAYS MINIATURE
TELEPHONE 170 Ω

SWITCHING
RELAY
MAGNECRAFT
96L 3.5 V
MINIMUM

quickly regain its normal emf.

In this system the rectifier will remain shorted when there is a sudden reversal of current because RL1 is not a polar relay. Since the reverse current through the cell array is only approximately 50 mA at 100°C and 7 V (plus some leakage current through the coolant), this current will allow RL1 to release. A sudden short at the cell side, however, will hold in the relay.

A fuse element removed from a 30A fuse will protect the battery in case of dead shorts. It was soldered because a fuse clip will add approximately 8 m ohms. A 10A fuse would afford more protection, but a standard fuse element of this size has a resistance of approximately 4 m ohms.

During testing of the system, it became clear that a dangerous condition existed at low flux levels because the pump needs approximately 2A starting current although it draws only about 0.7A down to about 3 volts during normal operation. Therefore, a transistor driven relay RL4 was provided to switch the pump over to the battery at low flux levels.

The pump motor is connected over A-B of the connector. The voltage drop over D4 will provide enough bias to pull in RL4 at about 100 mA, provided the voltage of the battery is over 3.5 V. RL2 switches off the starting circuit when enough charging current is available. A problem is to release RL4 at low currents since even in normal sunlight the cell array can supply about 30 mA and there is no load over D2. Therefore, R3 is switched in to replace the pump load allowing RL4 to release at approximately 60 mA. To prevent buzzing at low light levels, C1 slows down RL4. D3 was provided to insure pumping in case of poor contacts on RL4, and D4 prevents the current to the battery from bypassing D1. S1 can be

any low frequency silicon pnp transistor with the following specifications:

Dissipation = Min 100mW

I_C = Min 70mA

V_{CEO} = Min 8V

A 2N3134 transistor was used but a 2N3906 (an inexpensive plastic transistor) works just as well. Reverse leakage from the battery to S1 when the system is off is below $1\mu A$. By means of a switch on the pump cover, the pump motor can be switched to direct battery operation ("BAT") during filling and testing of the system. Table 2 gives a survey of the electrical losses of the system.

TABLE 2
ELECTRICAL LOSSES

Losses Caused By:	Series R	Loss at 2A		Loss at 6A
		Before Switching	After Switching	
	<u>m</u>	<u>Watts</u>	<u>Watts</u>	<u>Watts</u>
Wiring in cell array (calculated)	15.6	.062	.062	.94
Connection wires (40 ft. No. 6 wire)	16			.96
Rectifier D1	--	3.2	0	
RL2 max. contact R + wiring	3.0	--	.012	.18
RL3 coil	--	.19	0	
RL1 coil	1.2	.005	.005	.072
Fuse element	1.6	.007	.007	.096
RL4 coil	--	.30	0	
R3	--	2.5	0	
R4	--	.033	0	
Pump motor (at 7 volts)	--	4.6	4.6	4.6
Total Loss		10.9	4.7	6.9

It is possible to drive a moving coil meter to measure the output current without additional loss by using the voltage drop over a connection wire from the array to the electrical control box. A 1mA meter with a 50 mV full scale voltage drop would experience little temperature effect since its spring resistance is small compared with the resistance of the coil; and therefore the temperature coefficient of the meter would approximately match that of the wire.

The electrical control system could be modified in the following ways to improve the reliability:

1. A thermostatic switch mounted in the array could be used to replace Q1 and RL4.
2. A polarized current relay with low contact resistance could replace RL1 and RL2.
3. A low resistance circuit breaker could be used instead of the fuse.
4. For a safer system, a shutter arrangement in front of the array with solenoid triggering by a thermostatic switch would be valuable in case of cooling system failure.

F. ARRAY CONSTRUCTION

Each cell with a connection wire on the top was soldered to its individual heatsink as shown in Figure 5. Since it is important that the cells be heated for as short a period as possible, because of diffusion of the plating out of the cell into the solder, the connection wire was soldered on the cell concurrent with the soldering of the cell on a heatsink. The heatsink was clamped in a jig with the cell and wire underneath. The parts were held in place with glass strips and clamped from two sides, while the heatsink was held against the cell with a clamp between the pins in the middle of the heatsink. The jig was turned over and the heatsink was heated from the side with a 200 watt iron. As soon as the solder flowed, the pins were immersed in water for fast cooling. The 18 cells were then placed in a rectangular frame and mica was positioned around the edges of each heatsink for electrical insulation. The cells were molded in the frame with a low viscosity epoxy resin (Stycast 2651MM, Emerson and Cuming, Inc.). Figure 17 shows both sides of the frame and cells after molding. During casting an RTV seal was provided at the cell side. This was necessary because the epoxy must be thin enough to run between the heatsinks, and therefore it easily runs along the cell surface where it is difficult to remove. The RTV seals well and can be scraped off easily if wetted with petrolene. The epoxy should be poured over the pins to provide a protective coating against electrolytic corrosion. This was not done in the breadboard array and corrosion was evident after a few hours of operation. This problem was relieved by applying a thin coating of spray RTV to the pins.

Electrical connections were made between the wire from the top of each cell to a pin on the adjacent cell. The positive connection to the array

was made to the frame and the negative connection to the extended pin shown in Figure 17. The frame was screwed to the array base which included the water inlet and outlet connections. Figure 18 shows the complete array with an aluminum radiation shield used to protect the sides of the array from stray radiation.

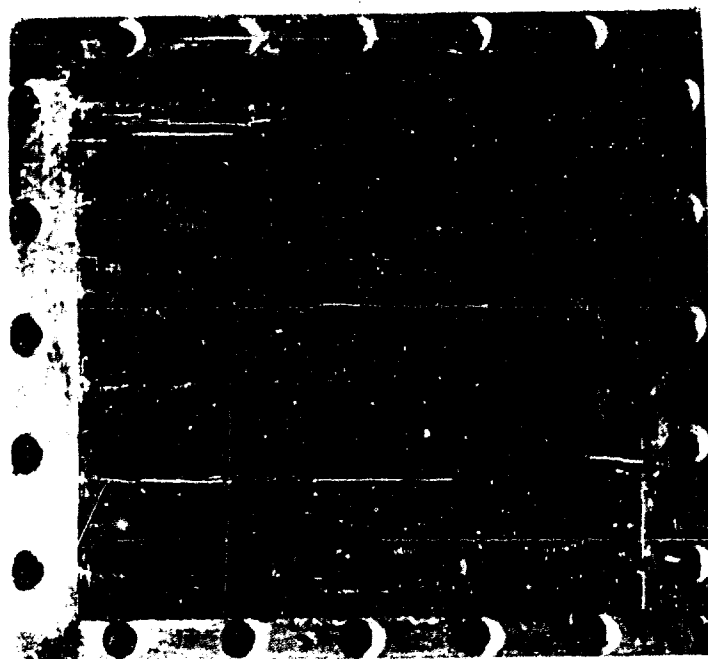
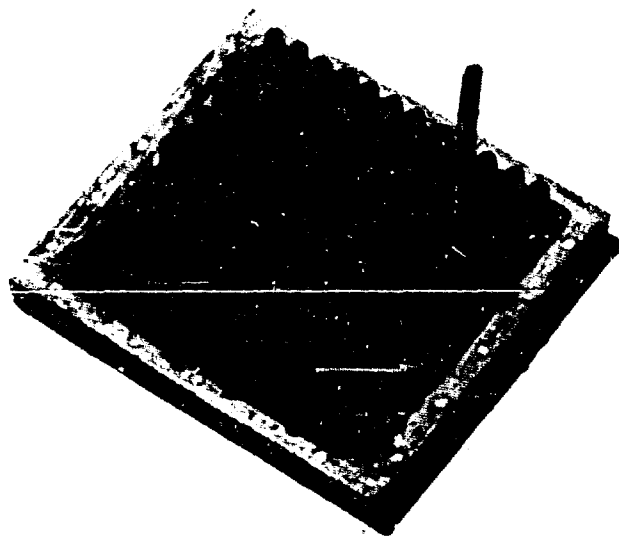
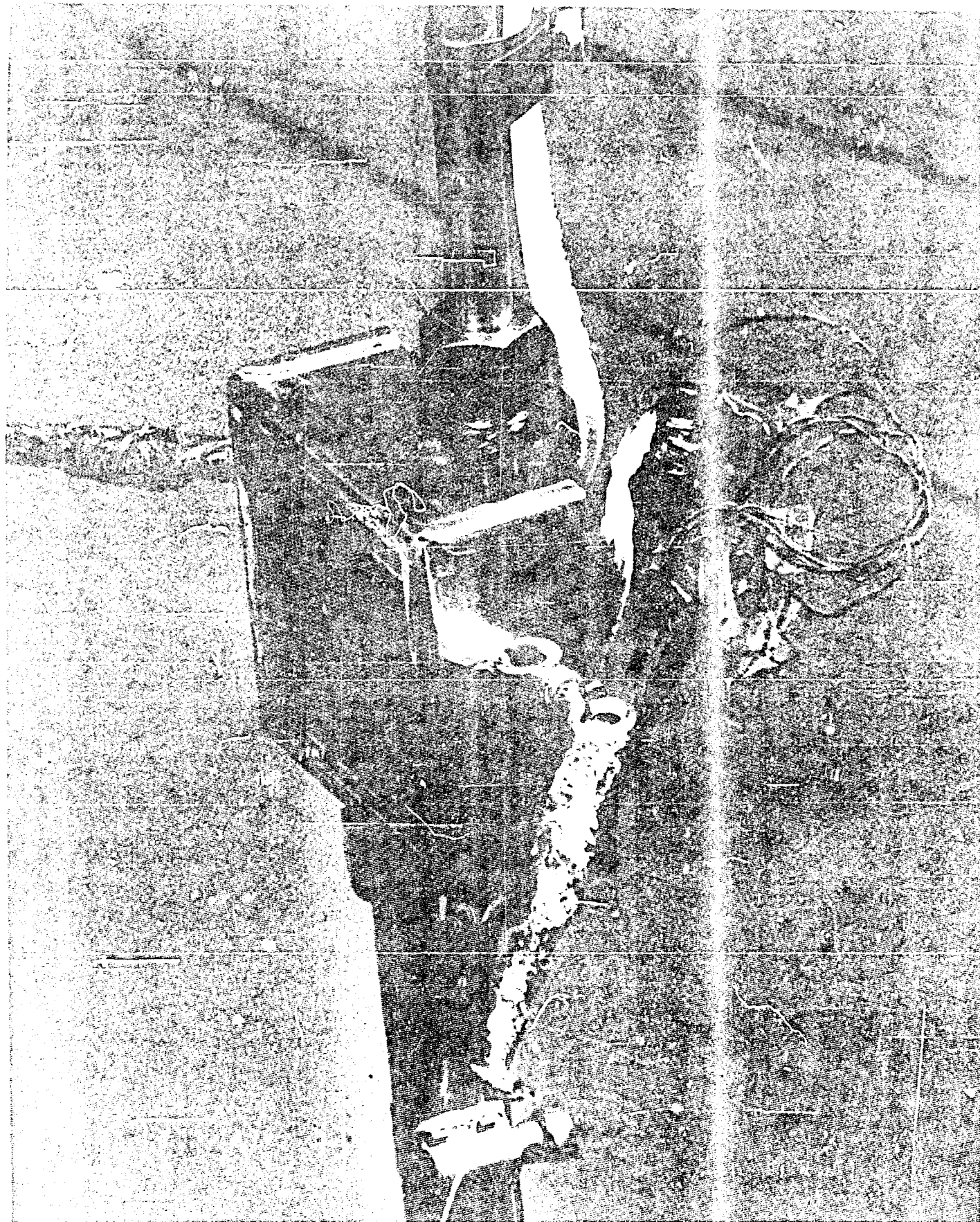


FIGURE 17. FRONT AND BACK VIEWS OF CELLS AND FRAME



Not Available Co FIGURE 16. CELL ARRAY

G. SYSTEM EXPERIMENTS

1. General Description

The Solar Energy Laboratory's heliostat tracking system, normally used with a solar furnace, was used to directly track the sun with the mosaic reflector. For this purpose, some heliostat mirrors were removed and the reflector was mounted on the heliostat panel. The tube with tracking sensors which normally is mounted on the furnace was mounted on the heliostat. An overall view of the system is shown in Figure 19. The tracking tube was adjusted so that the projected light pattern from the reflector was positioned symmetrically around the middle of an aluminum plate mounted in front of and centered with the cell array. Subsequent measurements with a flux probe (a small cell cut from a 30-gridline cell and mounted on cooling tubes) enabled a further small improvement in positioning to be made.

The following is a chronological account of the experiments and the difficulties that were encountered with the cell array.

- | | |
|---------|---|
| Oct. 13 | A voltage-current and a voltage-power curve were obtained which showed a maximum output of 40 watts. A short occurred between 2 cells and the frame after 3 hours' running time. It was found that the internal plating in the capsule (silver on brass) was flaking off (by electrolytic corrosion) and was touching pins. The capsule was sandpapered inside and coated with RTV silicone rubber. |
| Oct. 15 | During 3 hours' running time while charging a battery, a gradual decrease in current was observed. Also, the current was fluctuating with an amplitude of up to $\pm 1/2$ amp. A slight leakage of water between the |

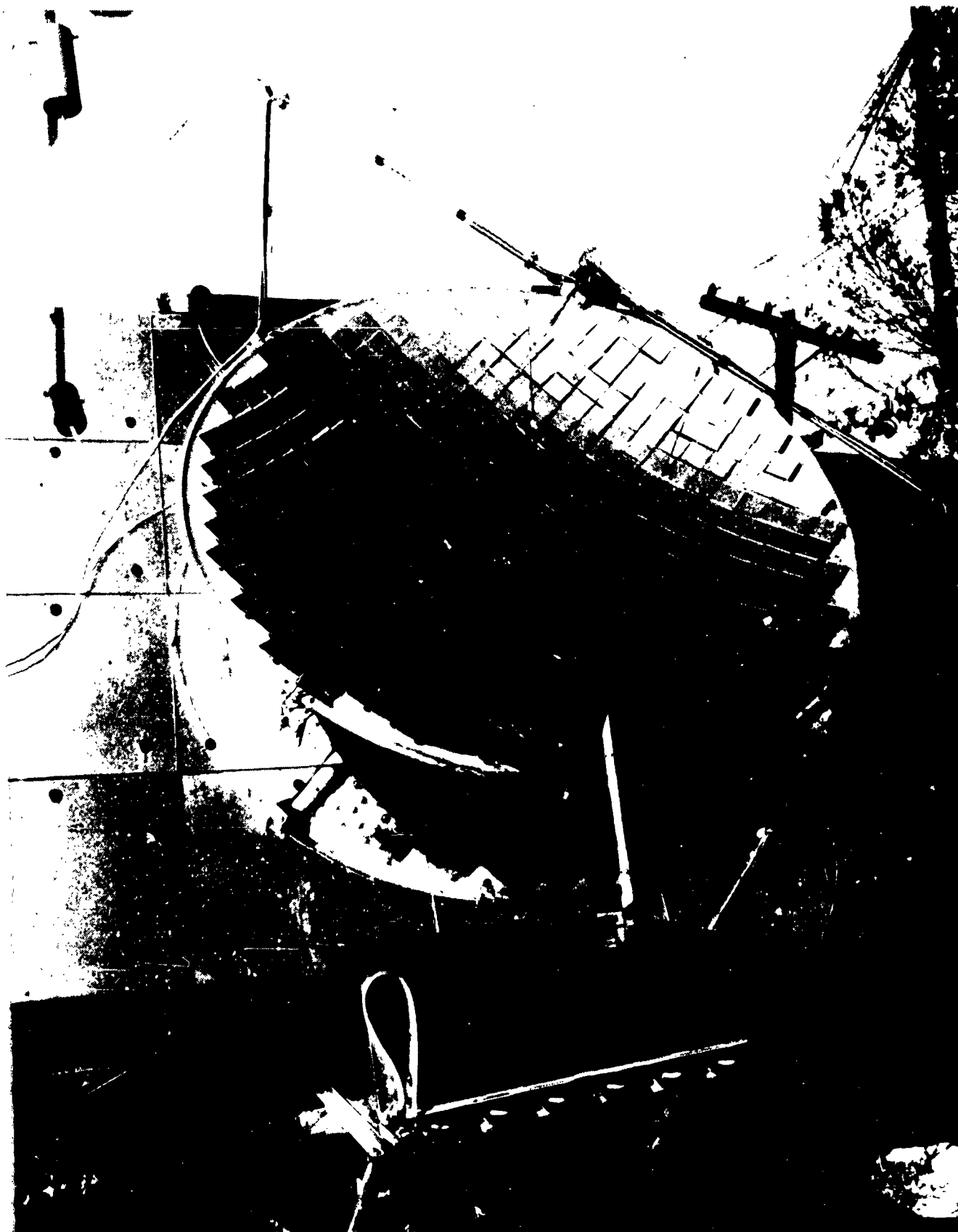


FIGURE 19. OVERALL VIEW OF SYSTEM

epoxy and frame at the sides parallel to the coolant flow was evident. At the end of the period, shorts were measured between some cells and the frame where water had leaked, and it was assumed that corrosion products had caused the short.

The array was disassembled and the cells were removed from the frame by sandblasting away the epoxy around the frame and sawing the frame into two pieces. The frame was repaired by silver solder and a shoulder was provided all around the frame to prevent further leakage. A shoulder had been originally provided on the two sides which did not leak. During disassembly, two cells were broken and were replaced by two new cells. The cells were then molded back into the frame with epoxy resin.

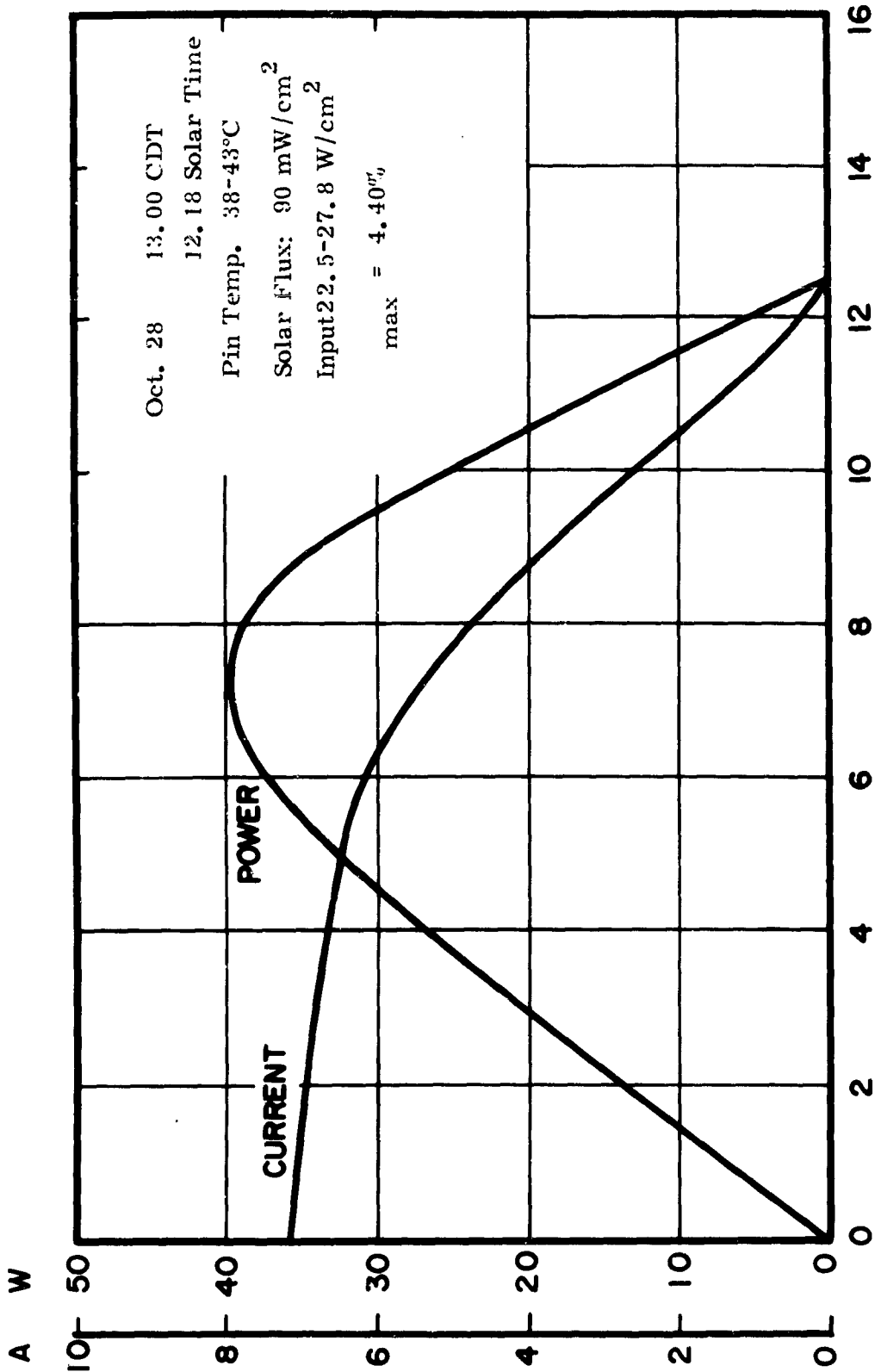
- Oct. 27 and 28: The charging current was not fluctuating any more. Current and power curves were taken on Oct. 28. A short developed after 7-1/2 hours total running time. It turned out that the foam plastic pad used as a gasket behind the pins had soaked up corrosion products and had become conductive. A film of RTV was applied on the pin side of a new pad and RTV was sprayed on the pins.
- Oct. 31, Nov. 1 and Nov. 2: No decrease in output was observed during 13-1/2 hours accumulated running time while the system was providing its own pumping power. One cell showed a crack at a corner, but this seemed to have no observable effect on the output. Since the broken part is still connected to the center strip, the break increases the total resistance of the cell but not the I_L output and only slightly reduces the efficiency.

2. Electrical Measurements

During October 27 and 28, current-voltage and power-voltage curves were obtained over the range of zero voltage to zero current. For these

measurements, a variable voltage power supply was connected in series with a measuring shunt over the output wires of the array. The voltage-current curve was traced on an x-y plotter from the output voltage, and the voltage drop over the shunt. The complete operating range of the array was measured by varying the output voltage of the power supply. It was necessary to connect a car battery in series with the power supply, with its polarity opposing the supply, in order to reach the open circuit voltage of the array.

The power curves were obtained by connecting the output of the array over the transmitting slidewire of a potentiometer recorder driven by the voltage drop over the shunt. The output from the wiper contact is then proportional to the product of current and voltage. The correct scaling was obtained by a variable resistor in series with the input to the slidewire. Errors caused by loading of the plotter input on the slidewire and of the slidewire on the array were calculated to be negligible. The electrical control box and pump were not in the circuit during these measurements. In Figures 20, 21 and 22, three measured current and power curves are given, taken on November 28. The actual temperatures of the cells were not known, but the temperatures halfway up the pins of three heatsinks in the middle of the array were measured and are calculated to be about 10°C lower than the cell temperature. Since the concentration ratio varied from about 250 to 300 (see Section D), the efficiency given with the curves was based on a concentration ratio of 275. In Figure 21, the pin temperatures are higher than in the other tests because the coolant flow rate was reduced and the heat exchanger was covered in an attempt to simulate high ambient temperature conditions. However, the low cooling flow rate results in large temperature gradients across the array which would not be present under high ambient



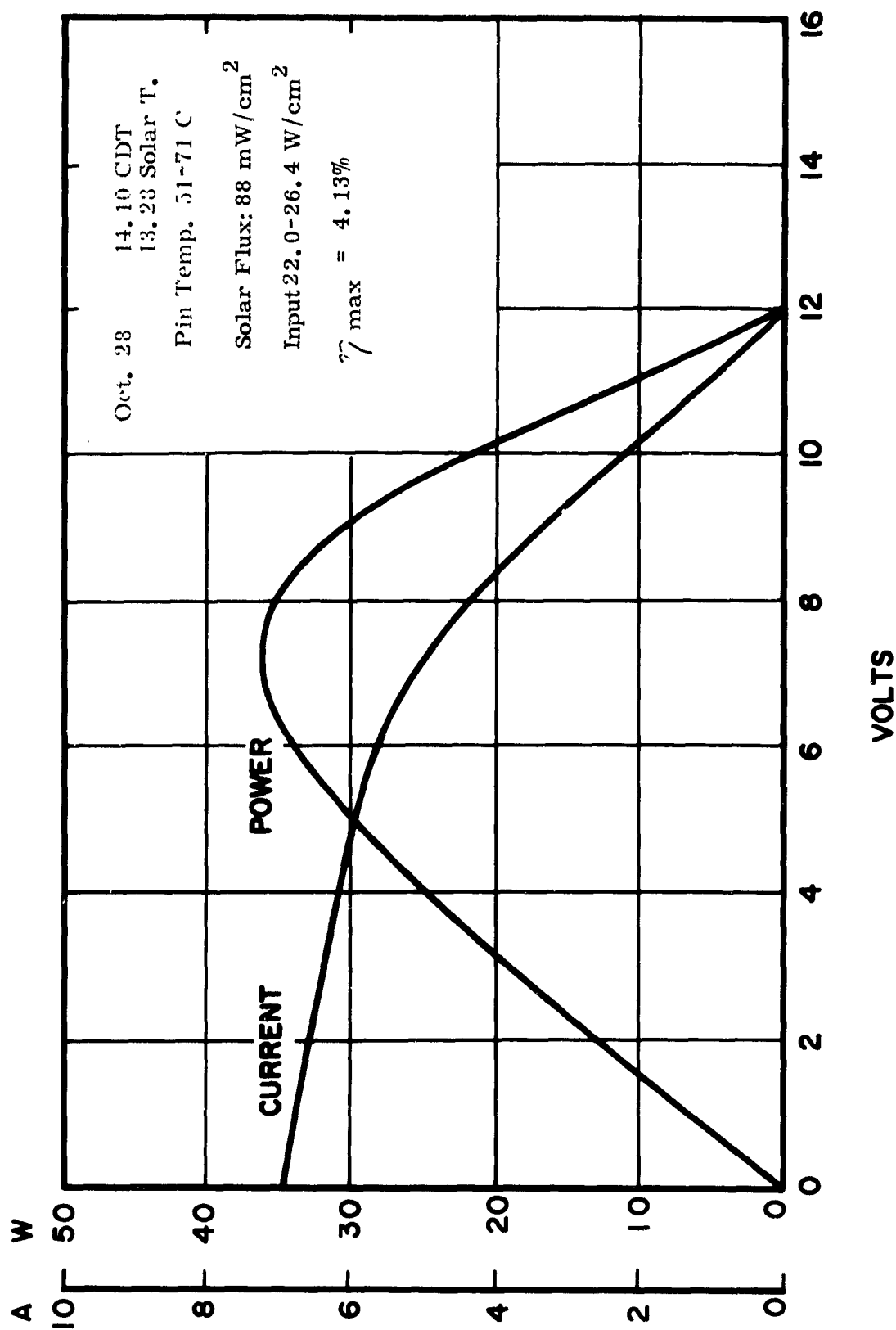
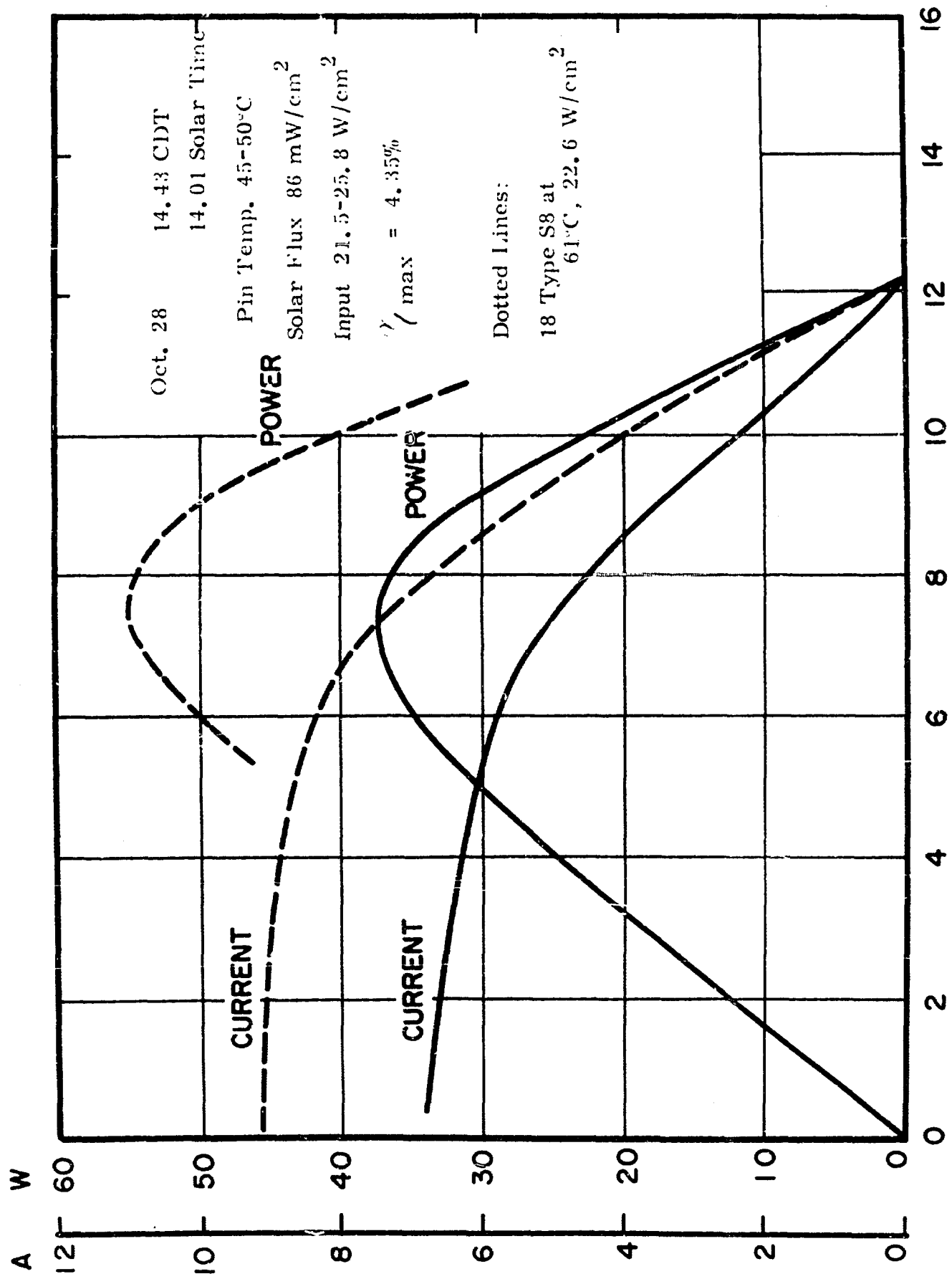


FIGURE 21. ARRAY CURRENT AND POWER VS. VOLTAGE AT 60°C



temperature operation.

In Figure 22, power and current curves for the array and for cell S8 (a thin 10-minute cell with 30 gridlines (see reference 4)) at a similar temperature and flux level and with the voltage multiplied by 18 to simulate the complete array are given for comparison. An array constructed from similar cells would generate over 50 watts at the given ambient radiation, and with uniform flux distribution. Improvements in the concentrator and cells should easily produce more than the 50 watt design level even at lower ambient radiation levels.

A nominal 6 V battery of about 100 Ah is well matched to this system in the range of maximum power since it will have a voltage at the terminals of between 6 and 8 volts.

H. CONCLUSIONS

It is possible to design and fabricate a high solar flux photovoltaic power system using 36 cm^2 of cell area and a solar flux of about 25 W/cm^2 which is capable of producing 40 watts of electrical power. Using a closed loop cooling system, 5 of the 40 watts are required for the pump motor. The individual cells used in the breadboard system had efficiencies which were considerably below the expected efficiency and also below previously tested cells. From measured and predicted cell characteristics, a system capable of producing between 60 and 70 watts of electrical power appears feasible.

I. RECOMMENDATIONS

It is recommended that studies of high solar flux cells be continued. This study should include a thorough comparison of predicted and measured cell efficiencies. In order to make meaningful comparisons, it will be necessary either to reduce the large variations in measured cell efficiencies caused by manufacturing techniques or to obtain large sample sizes for a statistical comparison. This would require close cooperation with a cell manufacturer.

The surface reflection characteristics of high flux cells should also be investigated. Long wave reflection coatings were not considered but should be studied as a means of increasing the cell performance. The advantages and disadvantages of plated contacts and sintered contacts should also be studied.

The use of a paraboloidal surface for the solar concentrator in conjunction with a flux distributor should be investigated as a means of obtaining a uniform flux distribution on the cell array. The use of a flux distributor would also permit larger tracking errors. The effect on the array output of a nonuniform flux distribution should be studied so that an optimum combination of flux distributor and concentrator can be designed.

APPENDIX

From the equivalent circuit of the generating part of a high flux cell with a distributed surface resistance and a distributed diode as shown in Figure 1A, the following equations can be derived:

$$\frac{di}{dz} = i_L - i_e \quad (1)$$

$$\frac{du}{dz} = -ir \quad (2)$$

Where $i_e = i_o(e^{Bu} - 1)$
 and $i =$ current at any point
 $i_L =$ light current per unit length
 $i_o =$ inverse saturation current of distributed diode per unit length
 $u =$ voltage at any point
 $r =$ surface resistance per unit length
 $B =$ exponent factor of distributed diode

Equations 1 and 2 have been numerically integrated on a digital computer from $z = 0$ to $z = Z$ to determine the generated voltage-current characteristics (1), (3). Since the shunt resistance is large for well made cells, it has negligible effect on the cell characteristics at high fluxes and can be neglected. In reference (1), the series resistance was included in the equivalent circuit to find the external voltage-current characteristics at high fluxes. In reference (3), the plating effect was introduced to account for an anomalous curvature of the external voltage-current relationship near the voltage axis.

For cells with negligible shunt resistance and plating effects, the following derivation is presented as a method for obtaining approximate values of the series resistance and distributed resistance from experimental current voltage curves at various solar fluxes.

In the 3rd and 4th quadrant of the current-voltage plane (the region of interest) the value of $u(o)$ (u at $z = o$) is always larger than or equal to $u(z)$. Thus the total integrated diode current will always be less than $i_o (e^{Bu(o)} - 1)$. If $u(o)$ is sufficiently small, so that $i_o (e^{Bu(o)} - 1)$ is small compared to i_L , then the distributed diode effect can be neglected and equations 1 and 2 simplified to:

$$\frac{di}{dz} = i_L \quad (3)$$

$$\frac{du}{dz} = -ir \quad (4)$$

In addition, if $u(o)$ is maintained constant, then equations 3 and 4 can be solved to obtain a single point on the cell voltage-current curve. The boundary conditions for equations 3 and 4 are then:

$$i(o) = o$$

$$u(o) = u^*$$

and the solutions are:

$$u(Z) = U = -i_L r \frac{Z^2}{2} + u^* \quad (5)$$

and

$$i(Z) = I = -i_L Z \quad (6)$$

If we now include the effect of the series resistance R_s the external voltage U_E will be:

$$U_E = \left(\frac{rZ}{2} + R_s \right) I + u^* \quad (7)$$

In a family of measured current-voltage curves with I_L as a parameter the region where the current approaches I_L is the region where the distributed diode effect becomes negligible. If the cells could be operated at various fluxes while $u(o)$ was maintained at u^* then the quantity $\frac{rZ}{2} + R_s$

could be obtained from $\frac{dU_E}{dI}$, since from Equation 7

$$\left. \frac{dU_E}{dI} \right|_{u^*} = \frac{rZ}{2} + R_s \quad (8)$$

Experimentally, it is difficult to measure $u(o)$ and consequently it is difficult to operate the cells with a constant $u(o)$ at various solar fluxes. An approximation to the constant $u(o)$ condition can be obtained by operating at points on the current voltage curves which have a small but finite deviation from I_L .

The total distributed diode current is the integrated value of i_e and in the region of I_L is a small quantity. The condition of a constant $u(o)$ for various fluxes would actually correspond to a deviation from I_L (i. e., the total diode current) which is a function of the operating current. But because of the exponential nature of the current voltage curves relatively large deviations from I_L occur over a small range of voltage and the fixed deviation condition will result in a relatively small error in maintaining a constant $u(o)$. Thus the gradient of the locus of points with a fixed deviation from I_L and with negligible diode effects is approximately equal to $\left. \frac{dU_E}{dI} \right|_u$. This line is shown in Figure 2A and is called the rho line.

An approximate value of R_s can be determined experimentally from the slope of the current-voltage characteristic at the open circuit voltage. If the plating effect and the shunt resistance can be neglected, then at zero current the distributed diode and resistance concept used in the generating part of the cell can be replaced by a single diode. With zero current the voltage at $z = 0$ will be the same as at $z = Z$, thus the magnitude of the distributed resistance will not affect the external voltage and the distributed diodes can be combined into a single diode. The equivalent circuit is then identical to that used for cells at normal fluxes. If the cell is operated near the open circuit voltage and thus with small currents, the single diod

concept will still be valid. The current and voltage relationships are then:

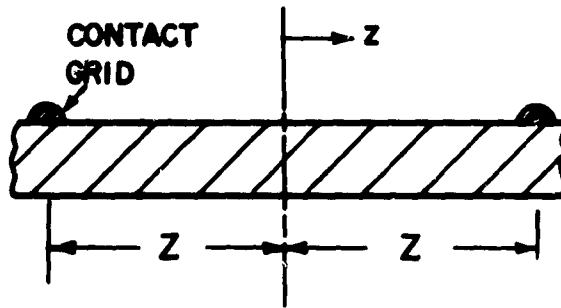
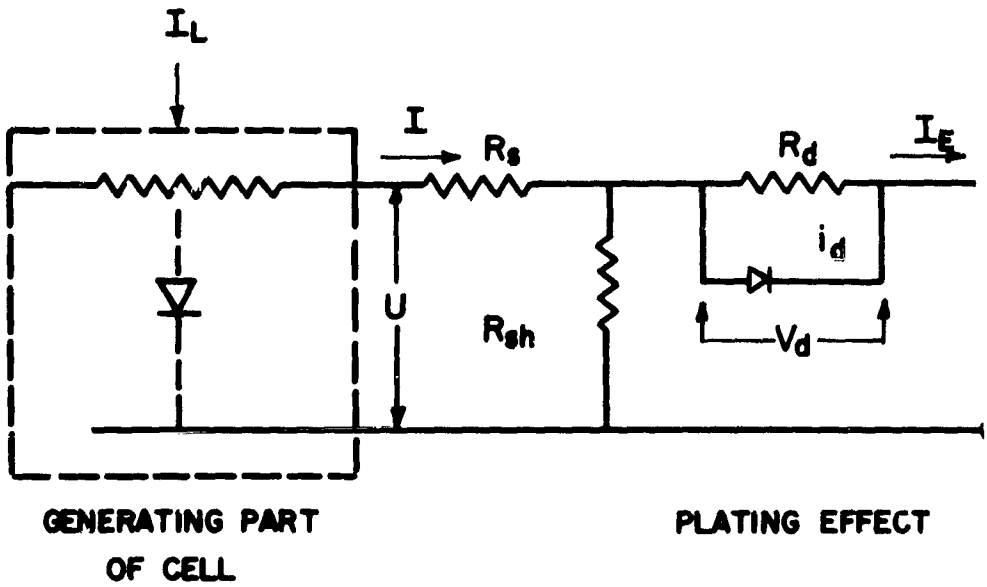
$$I = -I_L + I_o(e^{BU} - 1) \quad (9)$$

and
$$U_E = U + IR_s \quad (10)$$

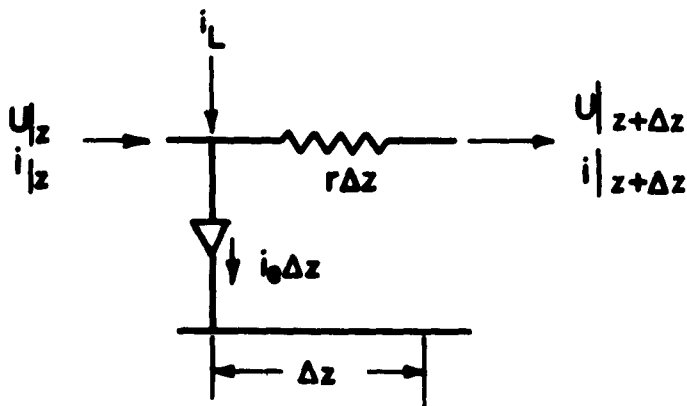
The slope of the voltage-current characteristic at $I = 0$ is then:

$$\left. \frac{dI}{dU_E} \right|_{I=0} = \frac{1}{R_s + \frac{1}{B(I_L + I_o)}} \quad (11)$$

Under high flux conditions, the quantity $1/B(I_L + I_o)$ is on the order of 10% of R_s . Thus from the slope of the voltage-current curve at the open circuit condition an approximate value of R_s can be determined.



CROSS SECTION OF CELL



EQUIVALENT CIRCUIT OF AN ELEMENT IN GENERATING PART OF CELL

FIGURE 1A. CELL EQUIVALENT CIRCUITS

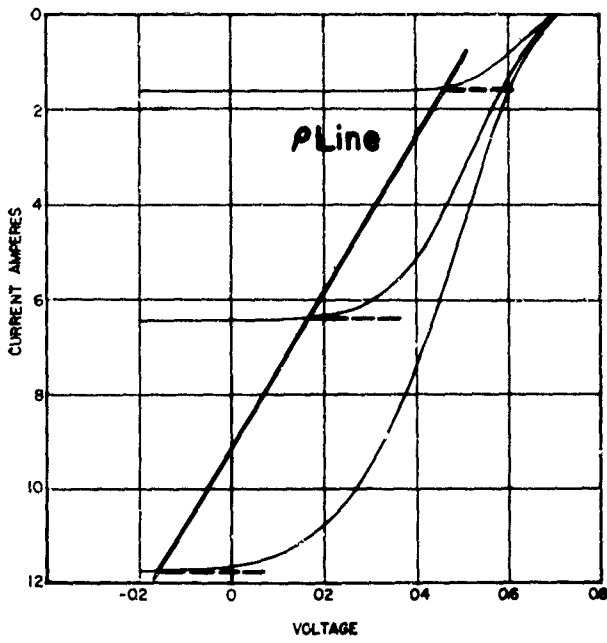


FIGURE 2A. RHO LINE

REFERENCES

1. Schoffer, P. and Pfeiffer, C. , "Performance of Photovoltaic Cells at High Radiation Levels," Journal of Engineering for Power, Trans. ASME, Series A, Vol. 85, 1963, p. 208.
2. Schoffer, P. , "High Power Density Solar Photovoltaic Conversion," Proc. of the 18th Annual Power Sources Conference, 1964, p. 166.
3. Schoffer, P. , Hartman, W. and Beckman, W. , Photovoltaic Power Systems Using High Solar Energy Fluxes, First Quarterly Progress Report, March 1 to May 31, 1964, University of Wisconsin, Solar Energy Laboratory.
4. Schoffer, P. , Hartman, W. and Beckman, W. , Photovoltaic Power Systems Using High Solar Energy Fluxes, Quarterly Progress Report No. 3, Sept. 1 to Nov. 30, 1964, University of Wisconsin, Solar Energy Laboratory.
5. McAdams, W. Heat Transmission, New York, McGraw-Hill, Third Edition, 1954.
6. Schoffer, P. , Hartman, W. and Beckman, W. , Photovoltaic Power Systems Using High Solar Energy Fluxes, Quarterly Progress Report No. 2, June 1 to Aug. 31, 1964, University of Wisconsin, Solar Energy Laboratory.

UNCLASSIFIED

Security Classification

DOCUMENT CONTROL DATA - R&D

(Security classification of title, body of abstract and indexing annotation must be entered when the overall report is classified)

1. ORIGINATING ACTIVITY (Corporate author) The University of Wisconsin, Madison, Wisconsin		2a. REPORT SECURITY CLASSIFICATION UNCLASSIFIED	
		2b. GROUP	
3. REPORT TITLE PHOTOVOLTAIC POWER SYSTEMS USING HIGH SOLAR ENERGY FLUXES			
4. DESCRIPTIVE NOTES (Type of report and inclusive dates) Final report Mar 64 - Nov 65			
5. AUTHOR(S) (Last name, first name, initial) Schoffer, P. and Beckman, W.			
6. REPORT DATE February 1966		7a. TOTAL NO. OF PAGES	7b. NO. OF REFS 6
8a. CONTRACT OR GRANT NO. DA28-043 AMC-00005(E)		9a. ORIGINATOR'S REPORT NUMBER(S)	
b. PROJECT NO. 106 22001 A 053			
c. Task No. -01		9b. OTHER REPORT NO(S) (Any other numbers that may be assigned this report)	
d. Subtask No. -11			
10. AVAILABILITY/LIMITATION NOTICES Distribution of this document is unlimited.			
11. SUPPLEMENTARY NOTES		12. SPONSORING MILITARY ACTIVITY U. S. Army Electronics Command Fort Monmouth, N. J. (AMSEL-KL-PA)	
13. ABSTRACT Experimental data is presented on the operation of a high solar flux power system. Using 18 one by two cm cells with 20 gridlines/cm and with a concentrated solar flux of about 25 W/cm ² , the system produced 40 watts of electrical power. Approximately 5 of the 40 watts are necessary for the cooling system pump motor. The expected net output of 50 watts was not obtained due to low cell efficiencies and nonuniform flux distribution. Probable reasons for the low cell efficiencies are discussed and a method for obtaining a more uniform flux distribution is presented. Tests on the individual cooling system components are also presented. (Authors)			

14. KEY WORDS	LINK A		LINK B		LINK C	
	ROLE	WT	ROLE	WT	ROLE	WT
High Intensity Solar Flux Silicon Photovoltaic Cells Solar Power Supply Cooling System Multi-grid contacts						

INSTRUCTIONS

1. ORIGINATING ACTIVITY: Enter the name and address of the contractor, subcontractor, grantee, Department of Defense activity or other organization (*corporate author*) issuing the report.

2a. REPORT SECURITY CLASSIFICATION: Enter the overall security classification of the report. Indicate whether "Restricted Data" is included. Marking is to be in accordance with appropriate security regulations.

2b. GROUP: Automatic downgrading is specified in DoD Directive 5200.10 and Armed Forces Industrial Manual. Enter the group number. Also, when applicable, show that optional markings have been used for Group 3 and Group 4 as authorized.

3. REPORT TITLE: Enter the complete report title in all capital letters. Titles in all cases should be unclassified. If a meaningful title cannot be selected without classification, show title classification in all capitals in parenthesis immediately following the title.

4. DESCRIPTIVE NOTES: If appropriate, enter the type of report, e.g., interim, progress, summary, annual, or final. Give the inclusive dates when a specific reporting period is covered.

5. AUTHOR(S): Enter the name(s) of author(s) as shown on or in the report. Enter last name, first name, middle initial. If military, show rank and branch of service. The name of the principal author is an absolute minimum requirement.

6. REPORT DATE: Enter the date of the report as day, month, year, or month, year. If more than one date appears on the report, use date of publication.

7a. TOTAL NUMBER OF PAGES: The total page count should follow normal pagination procedures, i.e., enter the number of pages containing information.

7b. NUMBER OF REFERENCES: Enter the total number of references cited in the report.

8a. CONTRACT OR GRANT NUMBER: If appropriate, enter the applicable number of the contract or grant under which the report was written.

8b, 8c, & 8d. PROJECT NUMBER: Enter the appropriate military department identification, such as project number, subproject number, system numbers, task number, etc.

9a. ORIGINATOR'S REPORT NUMBER(S): Enter the official report number by which the document will be identified and controlled by the originating activity. This number must be unique to this report.

9b. OTHER REPORT NUMBER(S): If the report has been assigned any other report numbers (*either by the originator or by the sponsor*), also enter this number(s).

10. AVAILABILITY/LIMITATION NOTICES: Enter any limitations on further dissemination of the report, other than those imposed by security classification, using standard statements such as:

- (1) "Qualified requesters may obtain copies of this report from DDC."
- (2) "Foreign announcement and dissemination of this report by DDC is not authorized."
- (3) "U. S. Government agencies may obtain copies of this report directly from DDC. Other qualified DDC users shall request through _____."
- (4) "U. S. military agencies may obtain copies of this report directly from DDC. Other qualified users shall request through _____."
- (5) "All distribution of this report is controlled. Qualified DDC users shall request through _____."

If the report has been furnished to the Office of Technical Services, Department of Commerce, for sale to the public, indicate this fact and enter the price, if known.

11. SUPPLEMENTARY NOTES: Use for additional explanatory notes.

12. SPONSORING MILITARY ACTIVITY: Enter the name of the departmental project office or laboratory sponsoring (paying for) the research and development. Include address.

13. ABSTRACT: Enter an abstract giving a brief and factual summary of the document indicative of the report, even though it may also appear elsewhere in the body of the technical report. If additional space is required, a continuation sheet shall be attached.

It is highly desirable that the abstract of classified reports be unclassified. Each paragraph of the abstract shall end with an indication of the military security classification of the information in the paragraph, represented as (TS), (S), (C), or (U).

There is no limitation on the length of the abstract. However, the suggested length is from 150 to 225 words.

14. KEY WORDS: Key words are technically meaningful terms or short phrases that characterize a report and may be used as index entries for cataloging the report. Key words must be selected so that no security classification is required. Identifiers, such as equipment model designation, trade name, military project code name, geographic location, may be used as key words but will be followed by an indication of technical context. The assignment of links, rules, and weights is optional.